DEPARTMENT OF DEFENCE
DEFENCE SCIENCE & TECHNOLOGY ORGANISATION
DSTO

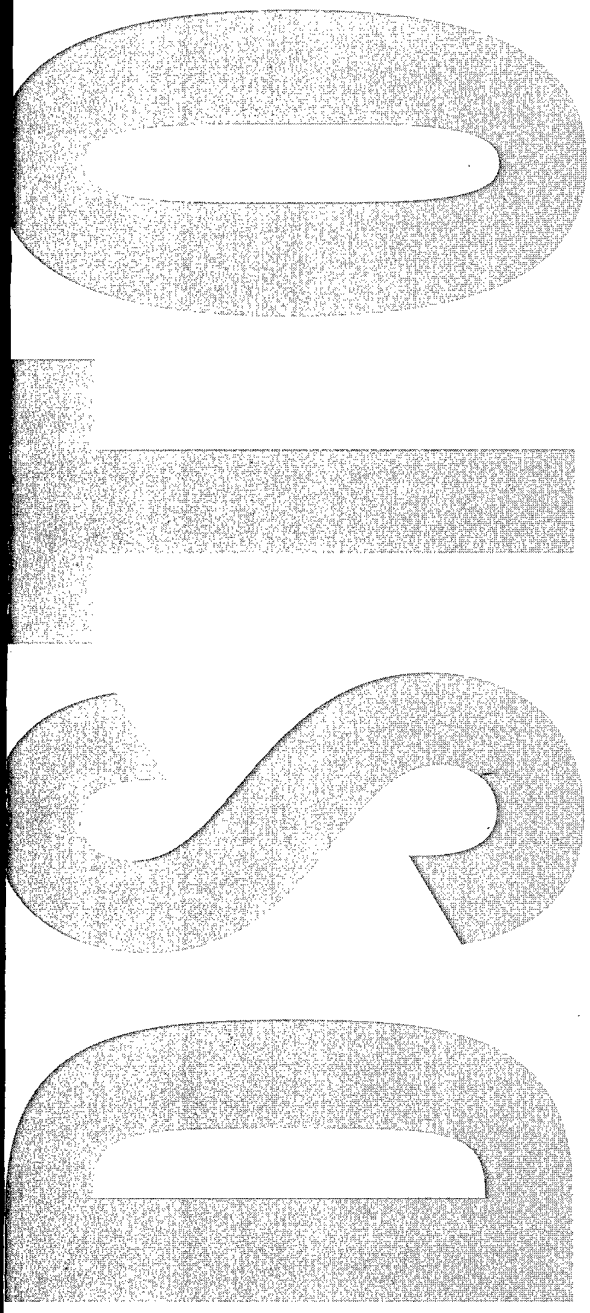

An Investigation of the Vibration Characteristics of the Eurocopter AS350B Main Rotor Gearbox Under Different Operating Conditions

Wenyi Wang

DSTO-TR-1217

DISTRIBUTION STATEMENT A
Approved for Public Release
Distribution Unlimited

20011203 205

An Investigation of the Vibration Characteristics of the Eurocopter AS350B Main Rotor Gearbox Under Different Operating Conditions

Wenyi Wang

Airframes and Engines Division
Aeronautical and Maritime Research Laboratory

DSTO-TR-1217

ABSTRACT

Different flight conditions can introduce complex changes to the vibration of helicopter transmissions, which may cause a vibration-based in-flight transmission diagnostic system to produce false alarms. An investigation into the vibration characteristics of the Eurocopter AS 350B main rotor gearbox under different operating conditions was conducted at AMRL. This investigation provided some in-depth understanding of the effects of different operating conditions, such as speed, torque and mast load, on the vibration of the gearbox. The analysis results showed that the effects of torque load were predominant and were dependent on operating speed and sensor locations, but that the effects of mast load were limited at most sensor locations. At the sensor location near the input shaft, the effects of torque and mast load on the vibration of the AS 350B gearbox were minimal.

RELEASE LIMITATION

Approved for public release

DEPARTMENT OF DEFENCE
DEFENCE SCIENCE & TECHNOLOGY ORGANISATION
DSTO

AQ F02-02-0341

Published by

DSTO Aeronautical and Maritime Research Laboratory
506 Lorimer St
Fishermans Bend Vic 3207 Australia

Telephone: (03) 9626 7000
Fax: (03) 9626 7999
© Commonwealth of Australia 2001
AR-012-029
October 2001

APPROVED FOR PUBLIC RELEASE

An Investigation of the Vibration Characteristics of the Eurocopter AS350B Main Rotor Gearbox Under Different Operating Conditions

Executive Summary

Different flight conditions and routine maintenance actions are regarded as common sources of false alarms for an in-flight fault diagnostic system of helicopter transmissions using vibration analysis. In order to distinguish the changes to gearbox vibration signatures produced by these factors from those induced by mechanical faults within the transmission gearbox, it is essential to understand how different operating conditions, such as speed, torque and mast load, affect the vibration of helicopter transmissions. This knowledge will determine whether the effects should be compensated for during fault diagnosis. For this purpose, an investigation into the vibration characteristics of the Eurocopter AS 350B main rotor gearbox under different operating conditions was conducted in the Helicopter Transmission Test Facility at AMRL. During the investigation, the raw vibration data were analysed statistically and spectrally.

The results showed that, at the nominal operating speed, the overall vibration level of the gearbox was predominantly affected by torque. The effects of torque on the spectral content of the vibration were also extensive and were location sensitive. The mast loads produced limited effects on the vibration level of the gearbox for three out of four tested sensor locations. The sensor location that was sensitive to mast load was on the side of the gearbox, where the transverse vibration was measured. The effects of mast load on the spectral content of the AS 350B gearbox vibration were limited. The sensor location least affected by torque and mast loading was near the input shaft to the gearbox.

Authors

Wenyi Wang
Airframes and Engines Division

Wenyi Wang received his Bachelor of Engineering and Master of Science degrees in China in 1982 and 1988, respectively. With the support of the prestigious Overseas Postgraduate Research Scholarship (OPRS) from Australian Commonwealth government, he got his PhD degree in mechanical engineering from University of New South Wales in 1996. From 1982 to 1998, Wenyi was employed as an Associate Lecturer and Lecturer at Wuhan University of Technology in China, the Australian Defence Force Academy, the Australian National University and Monash University. Since March 1998, he has been working with Aeronautical and Maritime Research Laboratory as a Research Scientist in the field of machine dynamics and vibration condition monitoring. Wenyi has published over 35 technical papers and reports.

Contents

1. Introduction

Different flight conditions and routine maintenance actions are regarded as common sources of false alarms for the in-flight fault diagnosis of helicopter transmissions using vibration analysis [1]. These factors can introduce complex changes to the vibration signatures of transmission gearboxes. In order to distinguish these changes from those induced by mechanical faults within the transmission, it is essential to understand how different operating conditions, such as speed, torque, and mast load affect helicopter gearbox vibration. This knowledge will determine whether these effects should and can be compensated for during the analysis of the vibration. Current analytical techniques simply acknowledge that gearbox vibration varies under different operating conditions, and thus limits analysis of the vibration to the periods when the operational parameters fall within certain bounds; e.g., 100 ±1 percent speed and 90 ±5 percent torque.

An investigation into the vibration characteristics of the Eurocopter AS 350B main rotor gearbox under different operating conditions was conducted in the Helicopter Transmission Test Facility (HTTF) at the Aeronautical and Maritime Research Laboratory (AMRL). This investigation provided in-depth understanding of the effect of different operating conditions on the vibration of this gearbox, preparatory to further research into the effects of mechanical faults.

2. Variable Operating Conditions Test

2.1 Test Conditions

The test was conducted in the HTTF. The vibration, lubricant pressure, and lubricant temperature of the AS 350B main rotor gearbox were measured under different speeds, torques, and rotor mast loads via various sensors. Four accelerometers were utilised for vibration measurement. They were mounted on the casing near the input shaft, the bevel gear and the ring gear (see Appendix A.1 for details).

The five test speeds chosen were 100%, 95%, 90%, 85% and 80% of the nominal operating speed, which is 6000 rpm at the input shaft (referred to as the turbine speed – nT). During the test, the torque on the rotor shaft (TR) was set to nine levels from 90% down to 10% (in steps of 10%) of the rated rotor torque, which is 9800 Nm. The vertical load (lift) applied to the mast was set to 0%, 50% and 100% of the maximum take-off weight (2,100 kg, or 20.6 kN). The horizontal load to the mast was set to 0%, 50% and 100% of one tenth of the maximum vertical load (2.0 kN), with five different force directions at the 2.0 kN load. These were 0°, 90°, 180°, 270° and 300° to the direction of input shaft (see Appendix A.2 for details). The load application points of two horizontal cylinders were 860 mm above the upper bearing of the gearbox. Therefore, the maximum applied horizontal load created a bending moment of 1720 Nm and a shear force of 2.0 kN in the mast at this point.

2.2 Automatic Test Procedure

The combination of the above conditions produced a large number of test steps (i.e., 5 speeds × 9 torques × 9 mast load combinations = 405 steps). In order to conduct the test efficiently, nine automatic test programs were created using the Excel program generator provided by the manufacturer of the HTTF (RENK of Germany), which is referred to as the Renk Program Generator (RPG). Each of these programs corresponded to one mast load condition. These RPG programs were then linked using the Renk Program Linker (RPL) to create the overall test procedure. The RPG and RPL are briefly described in the following sub-sections.

2.2.1 Renk Program Generator (RPG)

The RPG is an Excel macro program that can be accessed from the HTTF control software. With the RPG open, several operating parameters, such as the input speed, rotor torque, mast load, and the length of the running period can be edited. In this test, 3 minutes of running time were specified for each test step. Therefore, each RPG program consisted of 135 minutes of total test time, which was considered appropriate for a single test session. For each test session, a 13 minute warm-up period was allowed for the gearbox lubricant to reach the normal operating temperature, and a 4 minute run-down period was allowed for the loads to be reduced to zero prior to shut-down. An example of the RPG program is given in Appendix B.1. The torque loading arrangements for all RPG programs were identical. The differences in mast loading between the RPG programs are shown in Appendix Table B.2.

2.2.2 Renk Program Linker (RPL)

The RPL is also an Excel macro program, but it can only be accessed from the HTTF control software under the System (administrator) level. In the RPL, the various RPG programs discussed in the previous section were sequentially entered, along with the number of cycles for each RPG program. The RPL-filename field (including the path) on the top of the Excel table was entered and the RPL-set-cycles field was set to 100, although it could have been any positive integer. The other fields in the table were set to zero as they were automatically updated during the test. The RPL program for the test is included in Appendix B.2. The procedures for generating the automatic test programs and running the HTTF under the Automatic Mode are given in Appendix B.3.

2.3 Test Data

For each of the 405 test steps, 20 seconds of 16 sensor signals were recorded using a Metrum® RSR-512 DAT recorder. These included 4 tacho channels, 4 vibration channels, 2 torque channels, 4 mast load channels, a lubricant pressure channel, and a lubricant temperature channel. The detailed set-up of the Metrum recorder for each channel can be found in Appendix C.1. In order to analyse the signals in the powerful

Matlab® software package, 10 channels of each recording were sampled (8192 samples for each channel) using an Hewlett Packard E1432A VXI data acquisition board. Details of the sampled data can be found in Appendix C.2. These data were stored in Volts and were converted to engineering units using the calibration table shown in Appendix C.2.

3. Statistical Analyses of Test Data

3.1 Root-Mean-Square (RMS) Analysis of Vibration Data

The root-mean-square (RMS) values of the vibration signals were calculated under all test conditions. The results were stored in multi-dimensional Matlab arrays in conjunction with the mean measured values of the torque, and lubricant pressure and temperature signals. The arrays were saved in the Matlab file 'Vib_Rms.mat'. The structure of the multi-dimensional arrays can be found in Appendix C.3.

The RMS values of the vibration signals were plotted against the rotor torque (TR) at each of the five test speeds. These plots are shown in Figure 3-1 to Figure 3-5, where results from the various accelerometers are differentiated by colours and markers. In every plot, each accelerometer has 9 lines representing the 9 different mast load conditions; i.e., the 9 different RPL-stages as seen in Appendix B, Table B.3. As discussed in the following sections, it was found that the most dramatic change of RMS values with torque occurred at the Bevel-Side location at 95% speed (5700 rpm nT), where the vibration level changed from around 42g under 70% torque (6860 Nm TR), to 12g under 10% torque (980 Nm TR). At 80% speed (4800 rpm nT), the vibration levels at three out of the four sensor locations converged to tightly bound flat patterns.

3.1.1 Vibration at 100 Percent Speed (6000 rpm nT)

As shown in Figure 3-1, it was found that the RMS levels at all four sensor-locations changed non-linearly with torque, but tended to have stable trends above 50% torque (4900 Nm TR) - except for the Ring-Front location. At the Input-Pinion location, all the lines were tightly bound, indicating that the vibration at this position was not very sensitive to mast loads at this speed. The vibration levels at the Bevel-Front and Ring-Front locations also showed some insensitivity to mast loads except those at 80% torque (7840 Nm TR). It was obvious that the vibration at the Bevel-Side location varied significantly with the mast load at this speed – the variation was about 26% of the maximum level. Since 6000 rpm is the nominal input speed to the AS 350B gearbox, some more detailed vibration analyses at this speed are discussed in Section 3.2.1.

3.1.2 Vibration at 95 Percent Speed (5700 rpm nT)

With the input speed reduced to 95% (Figure 3-2), the results for the Input-Pinion location changed little from those at 100% speed. The results for the Bevel-Front

location were similarly unchanged below 40% torque (3920 Nm), but showed differences above this value, especially at 90% torque (8820 Nm TR). A detailed discussion about this result can be found in Section 3.2.2. Most notable were the results for the Bevel-Side location that had a completely different trend with respect to torque, and a different variance with respect to mast load from those shown in Figure 3-1. It was also found that, for the Bevel-Side location, the maximum vibration level at 95% speed (45g at 80% torque) was 1.4 times that at 100% speed (32g at 30% torque). This effect was possibly caused by the lateral vibration characteristics of the structure (e.g., a lateral structural resonance), which may suggest that this sensor is inappropriate for the purpose of consistent fault diagnosis. However, a vertically mounted sensor at this location may be less sensitive to this resonance.

3.1.3 Vibration at 90 Percent Speed (5400 rpm nT)

With the input speed further reduced to 5400rpm (Figure 3-3), there were some pattern changes for all four sensor-locations. At the Input-Pinion location, the vibration levels became flat (or insensitive) with respect to torque. At the Ring-Front location, the levels were slightly lower with higher torques (above 80%) than those shown at the previous speeds, and there was an increase of variance with mast load under 40% load. At the Bevel-Front location, the distribution pattern of the vibration levels differed substantially from those in Figure 3-1 and Figure 3-2, especially at both ends of the torque spectrum. Other anomalous behaviour exhibited by these characteristics is discussed in more detail in Section 3.2.2. The vibration levels at the Bevel-Side location changed again from Figure 3-2 with noticeable differences at both ends – higher levels at low loads, but lower levels at high loads.

3.1.4 Vibration at 85 Percent Speed (5100 rpm nT)

At 85% speed (Figure 3-4), the vibration levels at the Input-Pinion and Ring-Front locations decreased slightly from those at 90% speed. At the other two locations, the levels dropped significantly. Compared to the results at 90% speed, the trends of the vibration levels for each sensor location were similar, but the variances were quite different.

3.1.5 Vibration at 80 Percent Speed (4800 rpm nT)

The vibration levels at all four locations converged to tightly bound flat patterns at 80% speed (Figure 3-5). Compared to the results at 85% speed, the most dramatic change occurred at the Bevel-Side location where the maximum vibration level at 70% torque (6860 Nm TR) fell from around 25g to less than 10g, a reduction of more than 60%.

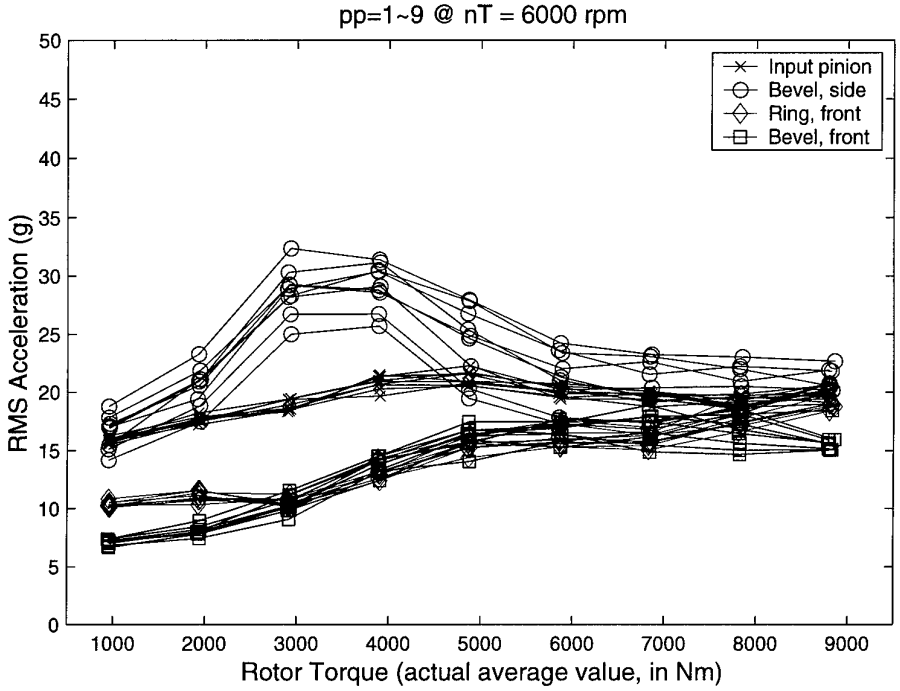

Figure 3-1. RMS acceleration vs. rotor torque (TR) at100% speed (6000rpm nT). For each sensor location, there are 9 different mast load conditions.

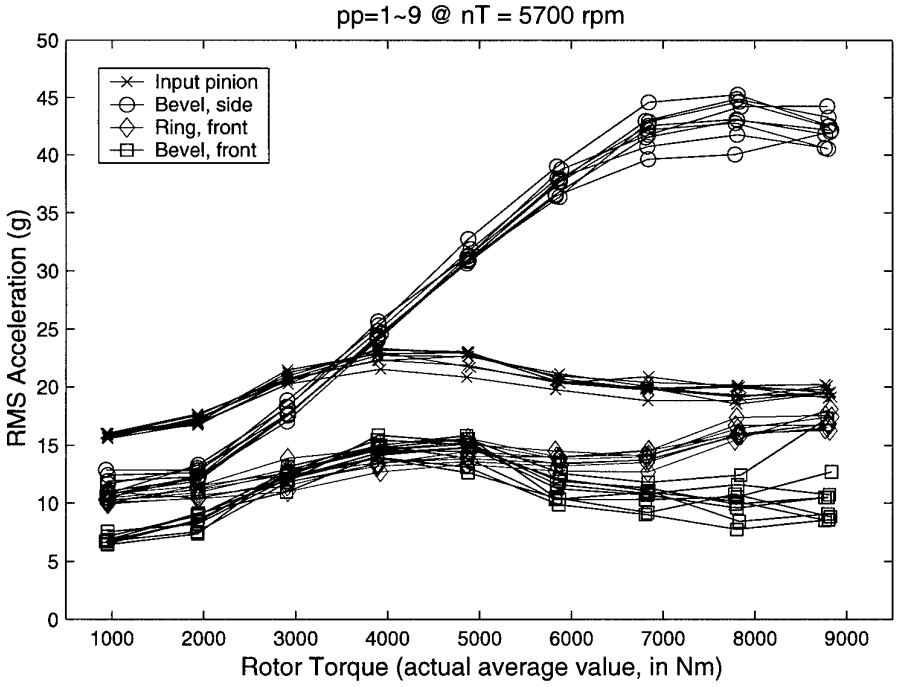

Figure 3-2. RMS acceleration vs. rotor torque (TR) at 95% speed (5700rpm nT).

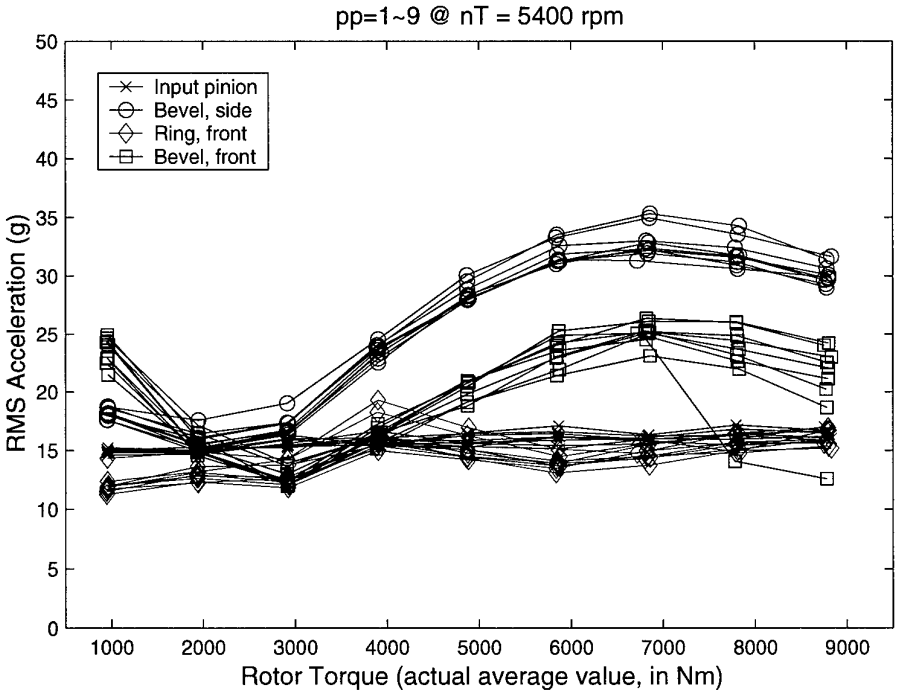

Figure 3-3. RMS acceleration vs. rotor torque (TR) at 90% speed (5400rpm nT). For each sensor location, there are 9 different mast load conditions.

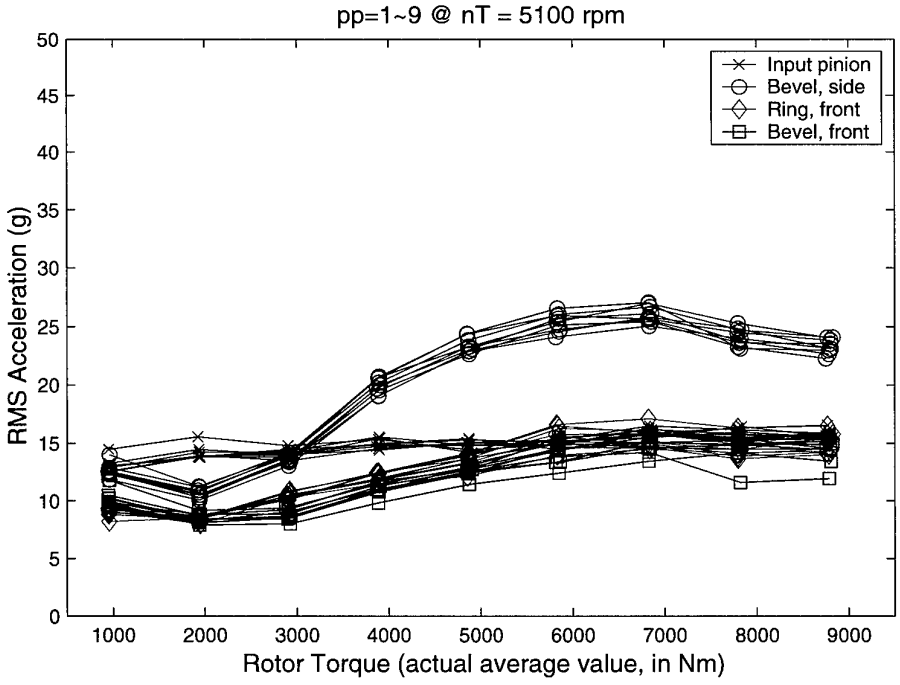

Figure 3-4. RMS acceleration vs. rotor torque (TR) at 85% speed (5100rpm nT).

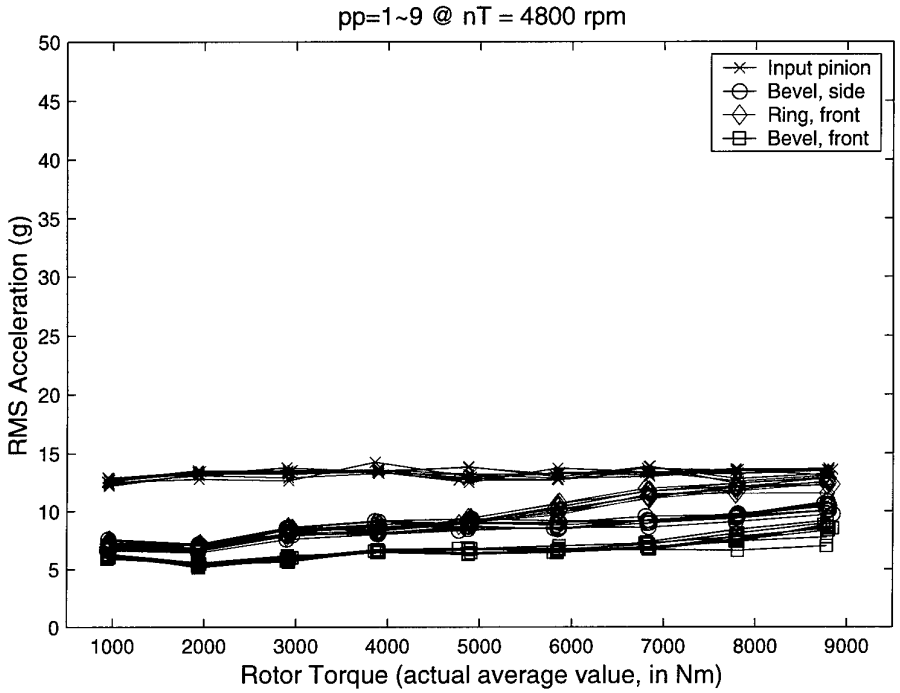

Figure 3-5. RMS acceleration vs. rotor torque (TR) at 80% speed (4800rpm nT).

3.1.6 Summary of RMS Analysis of Vibration Data

The major findings from the above discussion were:

- At the Bevel-Side location, the vibration levels were sensitive to both the speed and torque. However, they were only sensitive to the mast load at the input speed of 6000 rpm (100% speed). The largest variance occurred at the input speed of 5700 rpm (95% speed), where the vibration level varied from just above 10g at 10% torque to over 45g at 80% torque.
- At the Bevel-Front location, the vibration levels varied with torque at most tested speeds, but were only sensitive to the mast load in isolated cases; e.g., 90%~95% speed plus 80%~90% torque. The variations of the vibration levels with torque were heavily dependent on the speed and were highly non-linear at some speeds; e.g., 95% and 90% speed.
- At the Ring-Front location, the vibration levels were not sensitive to mast loads except at 90% speed around 40% torque (3920 Nm TR). For most tested speeds (except 90% speed), the overall vibration levels at this location were comparable to those at the Bevel-Front location.
- At the Input-Pinion location, there were fewer variations of the vibration levels than at the other sensor locations. The largest vibration variations with torque occurred at 100% and 95% speeds. At the lower (90%, 85% and 80%) speeds, the vibration levels were almost constant; i.e., little variation with respect to torque. Furthermore, it was found that the vibration levels at this location were not

sensitive to the mast load. This location may therefore prove to be most appropriate for consistent fault diagnoses.

- With an input speed of 4800 rpm (80% speed), the vibration levels at all four tested locations were the lowest among the five tested speeds, and were not very sensitive to the torque (except at the Ring-Front location) or to the mast load.

3.2 Mast-Load Sensitive Cases

In section 3.1, it was found that the most mast load-sensitive cases were the Bevel-Side location at 100% speed (see Figure 3-1), and the Bevel-Front location at the 95% and 90% speeds (see Figure 3-2 and Figure 3-3). In order to reveal the details of these situations, the data for these cases were extracted and plotted separately as shown in Figure 3-6 to Figure 3-8.

3.2.1 Case I: Bevel-Side Location at 100% Speed (6000 rpm nT)

As can be seen from Figure 3-6, the vibration levels at the Bevel-Side location were very sensitive to the torque at 100% speed, and the relationship was highly non-linear. The trends for all 9 mast-load conditions were similar, with the maximum levels at 30% or 40% torque and the minimum levels at 10% torque.

Under the different mast load conditions, the transverse vibration associated with no mast load (condition Vfc00, as indicated in Table B.2) was the largest, whereas the lowest level of transverse vibration was produced under the condition of full vertical and horizontal loads with a horizontal force angle of 180° (i.e., VfcFF2). The vibration also reached a similarly low level under the condition of full vertical and horizontal load with a horizontal force angle of 90° (condition VfcFF1). However, the similar conditions with horizontal force angles of 0° and 300° (VfcFF & VfcFF4) produced results similar to the no mast load condition. It is difficult to conclude exactly why this is so, however the higher levels of vibration may be associated with lower levels of system damping and vice versa.

3.2.2 Case II & III: Bevel-front Location at 95% and 90% Speeds

At the Bevel-Front location, where the sensor direction was aligned with the forward flight direction, the RMS vibration levels of the gearbox under the various mast loads were plotted against torque at 95% and 90% speed (5700 rpm and 5400 rpm nT), as shown in Figure 3-7 and Figure 3-8, respectively. It was found that the vibration levels at this location were only sensitive to mast load at high torques; i.e., above 50% torque. In addition, under the condition of full mast loads with a horizontal force angle of 270° (condition VfcFF3), the vibration levels at 80% and 90% torque were found to depart markedly from the general trends at both speeds. As a precaution, the data for these curious points were checked and confirmed as correctly recorded.

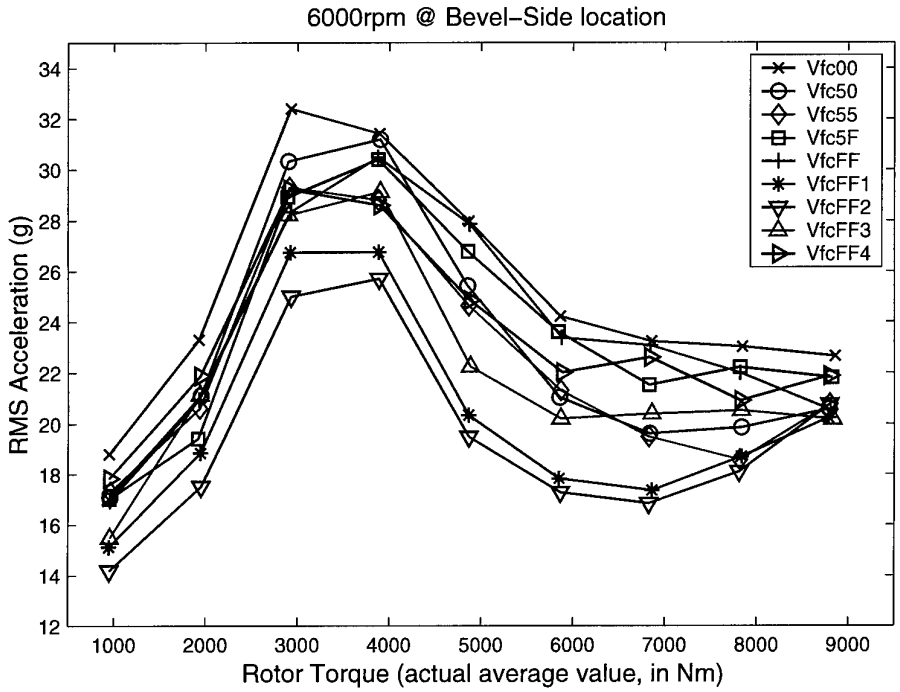

Figure 3-6. Mast-load sensitive case I: ***Bevel-Side*** *location with 100% speed (6000rpm nT). Each line represents a different mast load condition.*

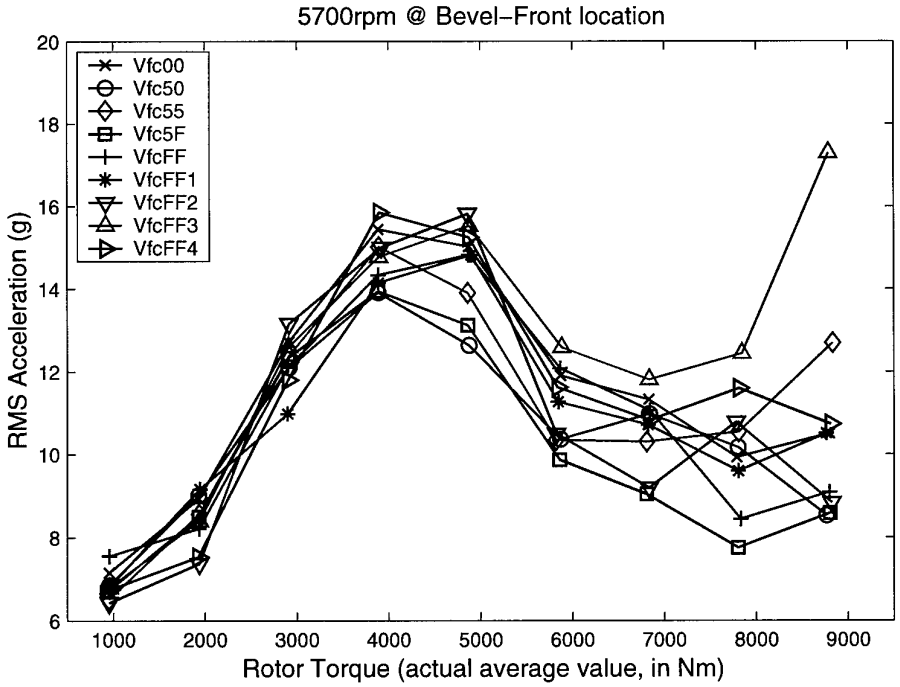

Figure 3-7. Mast-load sensitive case II: ***Bevel-Front*** *location with 95% speed (5700rpm nT).*

With regard to the vibration variation trends with torque, it was found that speed played a critical role. Comparing Figure 3-7 to Figure 3-8, it can be seen that the trends are almost reversed at these two speeds, and the absolute RMS levels at each torque are vastly different, except at 30% and 40% torque.

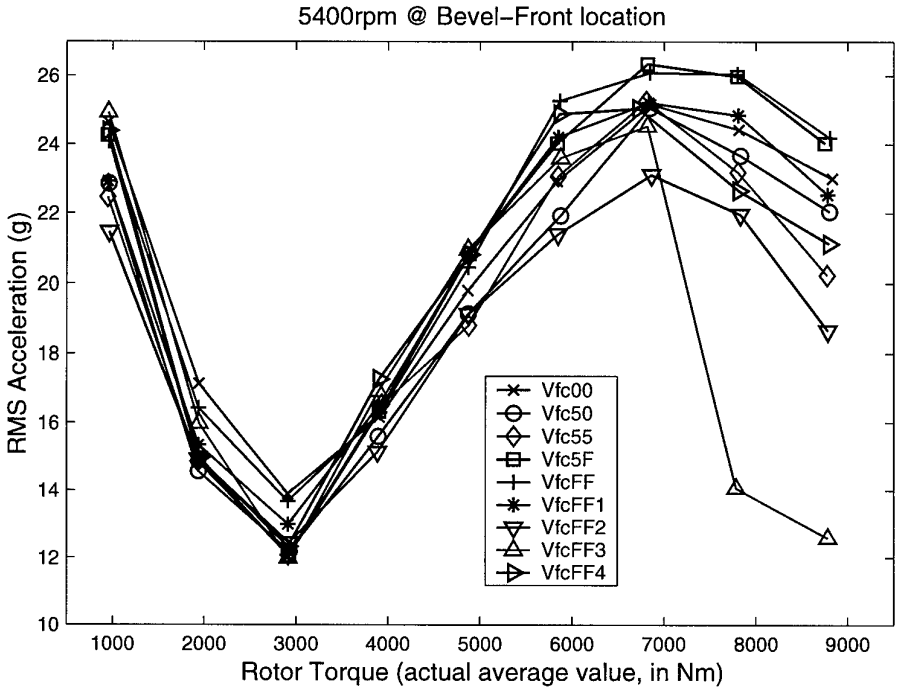

Figure 3-8. Mast-load sensitive case III: ***Bevel-Front*** *location with 90% speed (5400rpm nT).*

3.3 Analysis of Variance (ANOVA)

To statistically test whether the different operating conditions produced significant effects on the vibration levels of the AS 350B gearbox, the method of the Analysis of Variance (ANOVA) was used. ANOVA tests the null hypothesis of equal means between different groups of data samples by analysing or comparing the sample variances of those groups. A simple ANOVA can be accomplished by partitioning the total variance into the component that is due to true random error (i.e., within-group variance) and the components that are due to differences between the groups. The between-group components are then tested for statistical significance using the *F* statistic.

For the vibration data discussed in section 3.1, there were two major factors (torque & mast load) that influenced the vibration levels at each operating speed, thus a two-way ANOVA was conducted [2]. However, for simplicity, only the vibration data acquired at 100% speed (6000 rpm nT) were analysed, as this is the normal operating speed of

the AS 350B gearbox. For the purposes of the ANOVA, the vibration data files were equally partitioned into four 2048-sample segments (replications), and the RMS values for each segment were calculated. The structure of the extracted data matrices is described in Appendix C.4. The two-way ANOVA (a Matlab program is included in Appendix D.3) was then performed by partitioning the total variance of the RMS values into the components that were due to:

- torque,
- mast load,
- interaction effect (e.g., if the joint effect of torque and mast load taken simultaneously was different from the sum of their separate effects), and
- random error.

These were then tested by computing the ratio of the mean square of each group with the mean square of the random error, and were found to be significantly different if the value of this ratio exceeded the value of the $F_{a;\,v1,\,v2}$ statistic; i.e., if

$$F = \frac{MS_{group}}{MS_{error}} > F_{\alpha,v1,v2} = F_{critical} \qquad (1)$$

where a is the probability of falsely rejecting the hypothesis of equal means ($a = 0.05$ was used); $v1$ is the degrees-of-freedom of the group being tested; and $v2$ is the degrees-of-freedom of the random error. Also, for each computed F value, the probability of rejecting the null hypothesis of equal means if they were, in fact, the same, was calculated by replacing the inequality in Equation 1 with an equals sign and solving for a. The effects of the mast load were further analysed with two sub-analyses of: (a) the effects of horizontal and vertical load with torque at zero horizontal force angle, and (b) the effects of the angle of the horizontal load with torque at 100% mast load. The results of ANOVA are shown in Table 3-1, Table 3-2 and Table 3-3.

From Table 3-1, all sources of variance were found to be significant because the probabilities of accepting the null hypothesis were less than 0.05. From the third column of the table (% of total sum of squares), it can be seen that the variance due to torque was much greater than that due to mast load for all four sensor locations. Therefore, torque was the most dominant factor for the vibration levels of the gearbox at this speed (6000 rpm nT). It was also found that the levels of variance due to mast load, the interaction between torque and mast load, and error (i.e., within-group fluctuation) were very much dependent on the sensor locations.

At the Bevel-Side location (Table 3-1a), the variance due to mast load accounted for 14.78% of the total variance, which agreed with the findings in section 3.1.1 (see Figure 3-1). Further breaking-up the effect of mast load at this location with the sub-analyses, it was found that the variance due to horizontal and vertical loads with a horizontal force angle of 0° (see Table 3-2a) accounted for 5.91% of the sub-total variance. The variance due to the angle of horizontal force (see Table 3-3a) created the most effect, accounting for 16.15% of the sub-total variance. At the other three locations (Table 3-1b,

c and d), the effects of mast load on the gearbox vibration were no greater than 2% of the total. Notice that the corresponding sub-totals in the sub-ANOVA do not sum up to the total variances shown in Table 3-1, since the variance due to the interactions between the conditions in Table 3-2 and Table 3-3 were not included.

Table 3-1. Analysis of Variance (ANOVA) for the vibration data at 100% speed (6000 rpm nT) from the 4 sensor locations.

(a) Bevel-Side location (all conditions)							
Variation Source	*SS*	*% of Total*	*df*	*MS (SS/df)*	*F*	$F_{critical}$	*Probability*
Total	6279.00	100.00	323				
Torque	4932.00	**78.55**	8	616.50	1214.00	1.9766	0.0000
Mast Loading	928.00	14.78	8	116.00	228.40	1.9766	0.0000
Interaction	295.40	4.70	64	4.62	9.09	1.3642	0.0000
Error	123.40	1.97	243	0.51			

(b) Input-Pinion location (all conditions)							
Variation Source	*SS*	*% of Total*	*df*	*MS (SS/df)*	*F*	$F_{critical}$	*Probability*
Total	890.80	100.00	323				
Torque	765.40	**85.92**	8	95.68	367.60	1.9766	0.0000
Mast Loading	10.43	1.17	8	1.30	5.01	1.9766	0.0000
Interaction	51.72	5.81	64	0.81	3.11	1.3642	0.0000
Error	63.24	7.10	243	0.26			

(c) Ring-Front location (all conditions)							
Variation Source	*SS*	*% of Total*	*df*	*MS (SS/df)*	*F*	$F_{critical}$	*Probability*
Total	3345.00	100.00	323				
Torque	3111.00	**93.00**	8	388.88	787.20	1.9766	0.0000
Mast Loading	67.04	2.00	8	8.38	16.97	1.9766	0.0000
Interaction	47.33	1.41	64	0.74	1.50	1.3642	0.0157
Error	120.00	3.59	243	0.49			

(d) Bevel-Front location (all conditions)							
Variation Source	*SS*	*% of Total*	*df*	*MS (SS/df)*	*F*	$F_{critical}$	*Probability*
Total	4809.00	100.00	323				
Torque	4534.00	**94.28**	8	566.75	4329.00	1.9766	0.0000
Mast Loading	72.58	1.51	8	9.07	69.30	1.9766	0.0000
Interaction	170.30	3.54	64	2.66	20.33	1.3642	0.0000
Error	31.81	0.66	243	0.13			

Note: *SS* – sum of squares; *df* – degree of freedom; *MS* – mean square (= *SS/df*); *F* – F statistic (at α=0.05).

It is important to mention that, due to the large number of degrees of freedom, a very small percentage of the total sum of squares can still be seen as significant in a statistical sense. An effect is only statistically insignificant when the value of *F* is smaller than $F_{critical}$, or (equivalently) when the probability of rejecting the null hypothesis when it is true is greater than a given confidence level (i.e., 0.05 in these

analyses). In Table 3-2 and Table 3-3, the three underlined values in the *Probability* column indicate the cases that were statistically insignificant. These were: (a,b) the effects of horizontal and vertical mast load and its interaction with the torque at the Ring-Front location, and (c) the effect of horizontal mast load angle at the Input-Pinion location.

Table 3-2. Sub-ANOVA on the effect of horizontal & vertical mast loads at 100% speed

(a) Bevel-Side location (conditions Vfc00 ~ Vfc5F)							
Variation Source	*SS*	*% of Total*	*df*	*MS (SS/df)*	*F*	$F_{critical}$	*Probability*
Total	2875.00	100.00	143				
Torque	2561.00	89.08	8	320.20	483.50	2.0252	0.0000
Hor. & Ver. Mast Load	169.80	5.91	3	56.60	85.47	2.6887	0.0000
Interaction	72.71	2.53	24	3.03	4.58	1.6186	0.0000
Error	71.52	2.49	108	0.66			

(b) Input-Pinion location (conditions Vfc00 ~ Vfc5F)							
Variation Source	*SS*	*% of Total*	*df*	*MS (SS/df)*	*F*	$F_{critical}$	*Probability*
Total	371.10	100.00	143				
Torque	314.70	84.80	8	39.33	133.00	2.0252	0.0000
Hor. & Ver. Mast Load	8.73	2.35	3	2.91	9.84	2.6887	0.0000
Interaction	15.76	4.25	24	0.66	2.22	1.6186	0.0029
Error	31.95	8.61	108	0.30			

(c) Ring-Front location (conditions Vfc00 ~ Vfc5F)							
Variation Source	*SS*	*% of Total*	*df*	*MS (SS/df)*	*F*	$F_{critical}$	*Probability*
Total	1380.00	100.00	143				
Torque	1319.00	95.58	8	164.90	340.90	2.0252	0.0000
Hor. & Ver. Mast Load	1.54	0.11	3	0.52	1.06	2.6887	**0.3677**
Interaction	7.38	0.54	24	0.31	0.64	1.6186	**0.8993**
Error	52.24	3.79	108	0.48			

(d) Bevel-Front location (conditions Vfc00 ~ Vfc5F)							
Variation Source	*SS*	*% of Total*	*df*	*MS (SS/df)*	*F*	$F_{critical}$	*Probability*
Total	2281.00	100.00	143				
Torque	2203.00	96.58	8	275.30	2676.00	2.0252	0.000
Hor. & Ver. Mast Load	21.58	0.95	3	7.19	69.91	2.6887	0.000
Interaction	45.24	1.98	24	1.89	18.32	1.6186	0.000
Error	11.11	0.49	108	0.10			

Note: *SS* – sum of squares; *df* – degree of freedom; *MS* – mean square (= *SS/df*); *F* – F statistic (at a=0.05).

Table 3-3. Sub-ANOVA on the effect of angle of the (100%) vertical mast load at 100% speed

(a) Bevel-Side location (conditions VfcFF ~ VfcFF4)							
Variation Source	*SS*	*% of Total*	*df*	*MS (SS/df)*	*F*	$F_{critical}$	*Probability*
Total	3154.00	100.00	179				
Torque	2432.00	77.11	8	304.00	790.60	2.0076	0.0000
Angle of Ver. Mast Load	509.30	16.15	4	127.30	331.10	2.4387	0.0000
Interaction	161.00	5.11	32	5.03	13.08	1.5294	0.0000
Error	51.91	1.65	135	0.39			

(b) Input-Pinion location (conditions VfcFF ~ VfcFF4)							
Variation Source	*SS*	*% of Total*	*df*	*MS (SS/df)*	*F*	$F_{critical}$	*Probability*
Total	519.30	100.00	179				
Torque	457.800	88.16	8	57.22	246.90	2.0076	0.0000
Angle of Ver. Mast Load	1.329	0.26	4	0.33	1.43	2.4387	**0.2263**
Interaction	28.920	5.57	32	0.90	3.90	1.5294	0.0000
Error	31.290	6.03	135	0.23			

(c) Ring-Front location (conditions VfcFF ~ VfcFF4)							
Variation Source	*SS*	*% of Total*	*df*	*MS (SS/df)*	*F*	$F_{critical}$	*Probability*
Total	1954.00	100.00	179				
Torque	1798.00	92.02	8	224.70	447.60	2.0076	0.0000
Angle of Ver. Mast Load	55.20	2.83	4	13.80	27.48	2.4387	0.0000
Interaction	33.36	1.71	32	1.04	2.08	1.5294	0.0021
Error	67.78	3.47	135	0.50			

(d) Bevel-Front location (conditions VfcFF ~ VfcFF4)							
Variation Source	*SS*	*% of Total*	*df*	*MS (SS/df)*	*F*	$F_{critical}$	*Probability*
Total	2524.00	100.00	179				
Torque	2350.00	93.11	8	293.70	1915.00	2.0076	0.0000
Angle of Ver. Mast Load	46.13	1.83	4	11.53	75.21	2.4387	0.0000
Interaction	107.10	4.24	32	3.35	21.82	1.5294	0.0000
Error	20.70	0.82	135	0.15			

Note: *SS* – sum of squares; *df* – degree of freedom; *MS* – mean square (= *SS/df*); *F* – F statistic (at a=0.05).

3.4 Lubricant Pressure and Temperature Data

The mean values of the lubricant pressure data (8192 samples) were plotted against the torque at each speed, as shown in Figure 3-9. Not surprisingly, as the gearbox uses a geared pump, the pressure varied greatly with speed, and it was not particularly sensitive to either the torque or the mast load. It was found that the largest relative variation of the pressure with respect to the mast load was around 6.3% at 90% speed (5400 rpm nT) and 40% torque (3920 Nm TR). With respect to torque, the largest relative variation of the pressure was 8.3% at 80% speed and 30% to 40% rotor torque.

The HTTF uses the same transmission oil cooler as found in the AS 350B helicopter, and this cooler uses an electric fan that is configured to engage at 77°C and disengage at 68°C of the oil temperature. It was therefore not surprising to find that the average values of the 8192-sample temperature signals presented in Figure 3-10 circulated between the thermostat limits for the cooling fan. It can also be seen in this figure that the pressure was slightly sensitive to the temperature. This was probably caused by the viscosity of the oil falling slightly with increased temperature. The temperature circulation process was not dependent upon any of the other operating parameters; i.e., speed, torque and mast load (Figure 3-11).

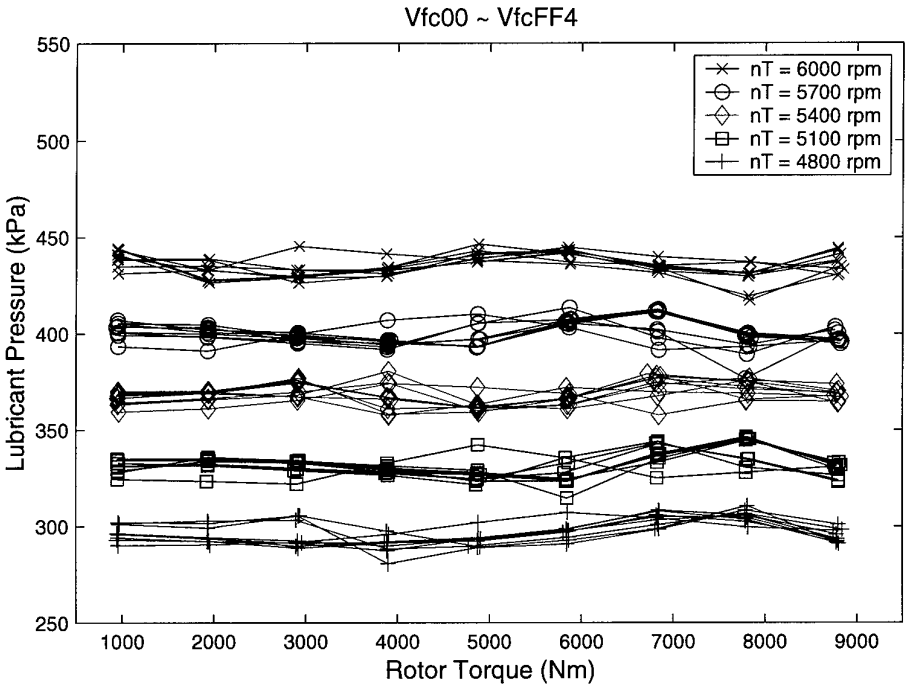

Figure 3-9. Lubricant pressure vs. rotor torque.

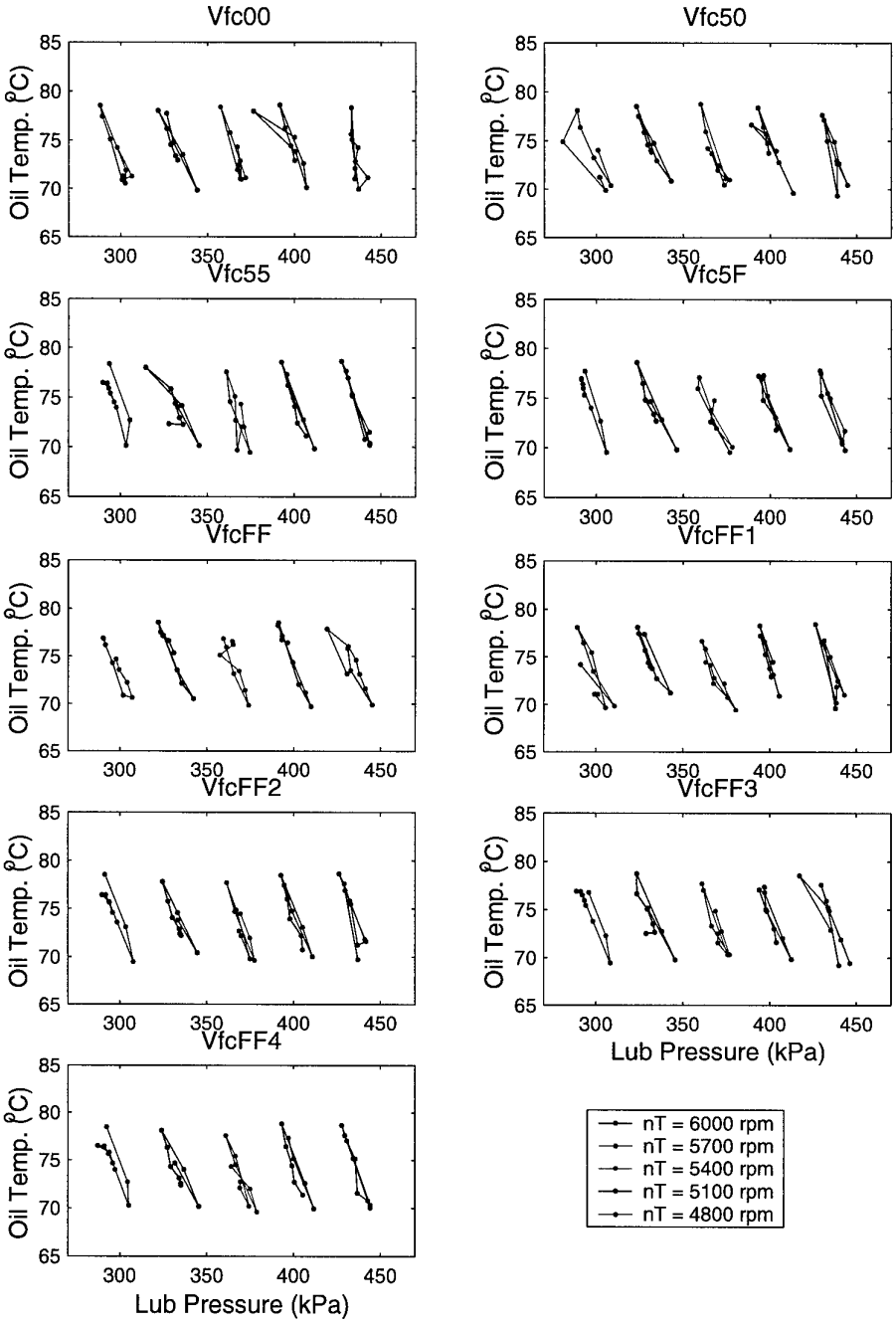

Figure 3-10. Lubricant temperature vs. pressure at various input speeds (nT)

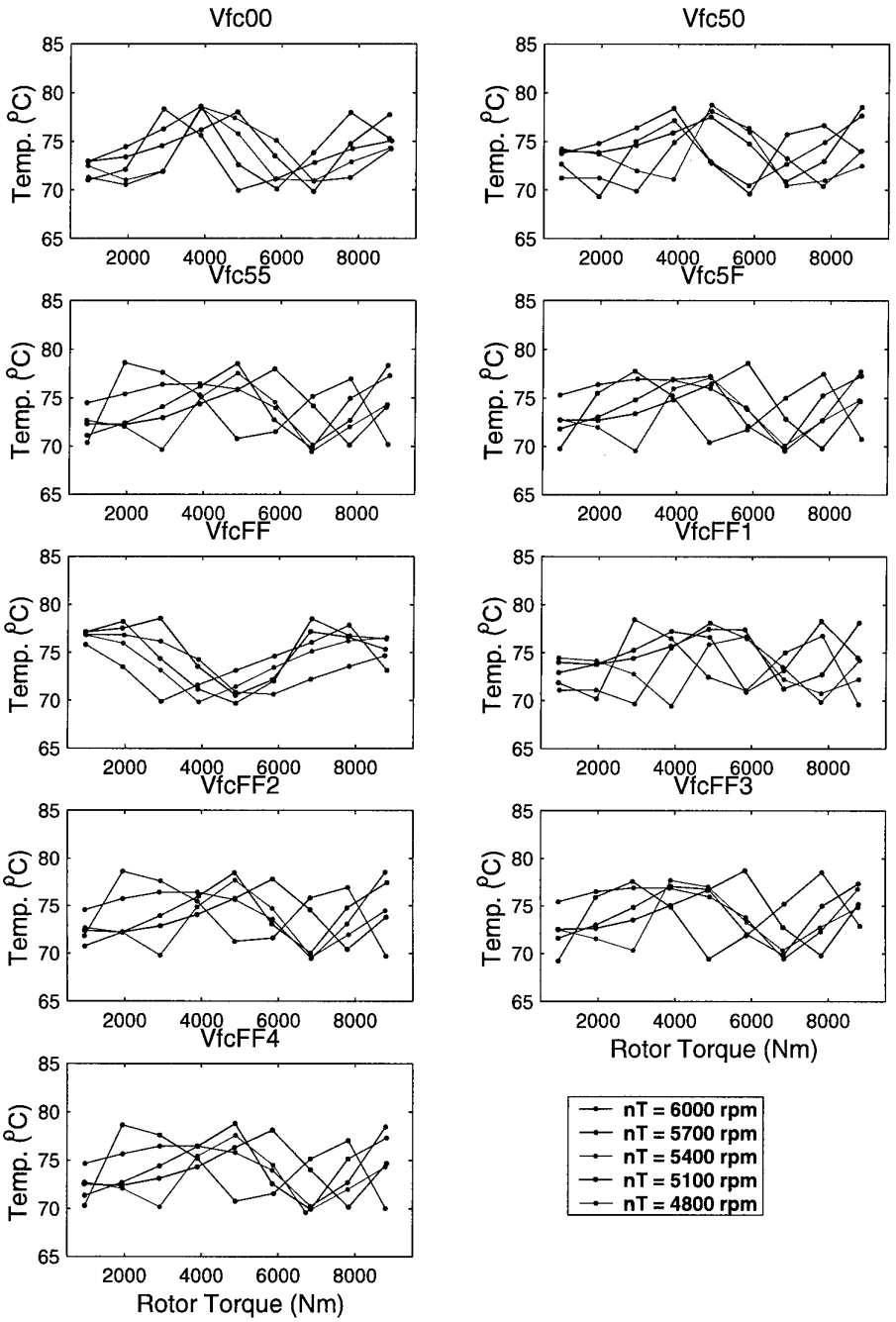

Figure 3-11. Lubricant temperature vs. rotor torque (TR).

4. Spectral Analyses of Vibration Data

This section presents the results of the spectral analyses of the vibration data. The power spectral density functions were calculated for all 8192-point vibration data files using Welch's method with a FFT length of 1024 points, an overlap of 512 points, and a Hanning window. The results along with a frequency index were stored in a Matlab data file – "Vib_PSD.mat", whose structure is described in Appendix C.5.

Prior to displaying the power spectra, the RPG-stages with the same speed were extracted from each RPL-stage (refer to Table B.2) and rearranged to form a descending order of the rotor torque; i.e., from 8820 Nm to 980 Nm, as shown in Table 4-1.

Table 4-1. Arrangement of load conditions

RPL-stage **1** *VFC00.RPG*				*RPL-stage* **2** *VFC50.RPG*				....	*RPL-stage* **9** *VFCFF4.RPG*			
8820	7840	...	980	8820	7840	...	980	.....	8820	7840	...	980
1	**2**	**...**	**9**	**10**	**11**	**...**	**18**	.....	**73**	**74**	**...**	**81**
Load conditions (vertical axis of the power spectral images)												

4.1 Power Spectral Images

The power spectra are displayed here as images, where the horizontal axis is frequency (in terms of input shaft orders) and the vertical axis represents the various load conditions. The power spectral magnitude is represented by colour intensity on a logarithmic scale. All the images are mapped to a uniform colormap of [0, 58] dB, where 58 dB is the highest level for all spectra – obtained from the Bevel-Side location at 95% speed. For the AS 350B main rotor gearbox, the gear meshing frequencies of the bevel gear stage and the epicyclic stage are 17 and 6.43 orders of the input shaft frequency, respectively (i.e., 1700 Hz and 643 Hz at 100% speed).

The power spectral images at 100% speed (6000 rpm nT) are shown in Figure 4-1. It is obvious that the harmonics of the bevel gear meshing frequency were dominant in all four sensor-locations. The harmonics of the epicyclic gear meshing frequency were, however, only visible in the images for the Input-Pinion and Ring-Front locations due to their close vicinity to the epicyclic stage. The largest harmonic component occurred at the Bevel-Side location, where the vibration was measured in the transverse direction (perpendicular to the forward flight direction). At the Input-Pinion location, there was a structural resonance around 13,600 Hz (136 orders of the input shaft frequency at this speed) with an intensity of approximately 40 dB (refer to the colorbar). The differences of the spectral content between the different mast load conditions (RPL-stages) are not readily discernable in these images.

With the operating speed reduced to 95% (5700 rpm nT), the magnitude at the bevel gear meshing frequency at the Bevel-Side location increased to about 58 dB (Figure 4-2c). However, the second harmonic of this frequency at the same location was weaker than that at 100% speed.

With the speed further reduced to 90% (5400 rpm nT), the most obvious changes were that the magnitudes at the Bevel-Side and Input-Pinion locations became weaker, and at the Bevel-Front location became stronger (Figure 4-3).

For the other two tested speeds (Figure 4-4 and Figure 4-5), the spectral magnitudes were generally decreasing with the speed. However, one interesting finding was that the 3rd harmonic component of the bevel gear mesh frequency (51 input shaft orders) at the Ring-Front location emerged as the strongest component at 85% speed (5100 rpm nT).

4.2 Variation of Spectral Components with Mast Load

To further reveal the variation in the amplitudes of the spectral components with different mast loads, some of the high-power spectral components were more closely examined.

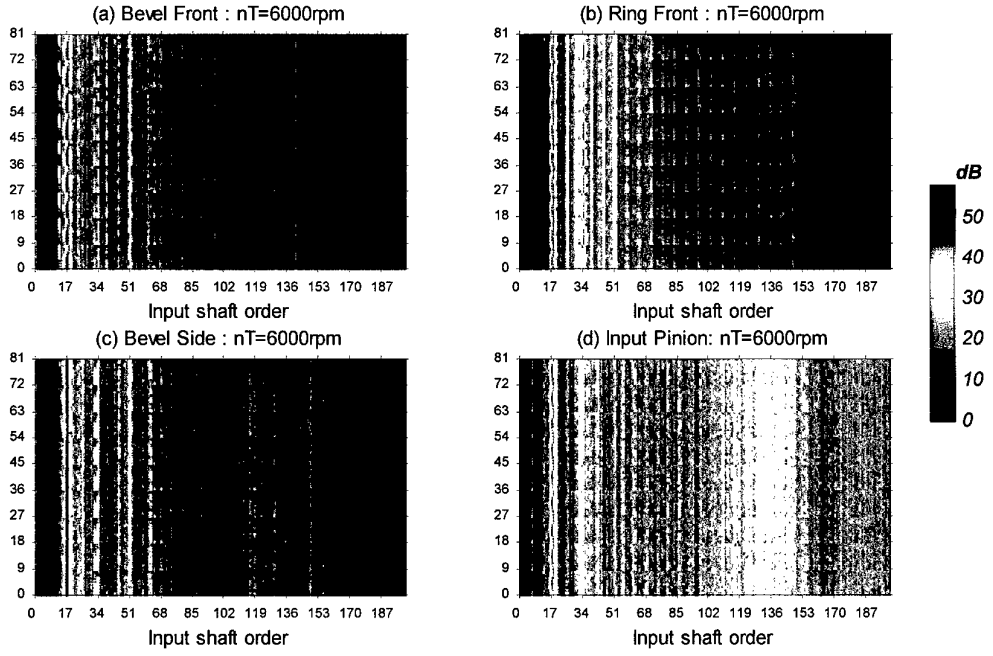

Figure 4-1. Power spectral images of the vibration signals at 100% speed (6000 rpm nT).

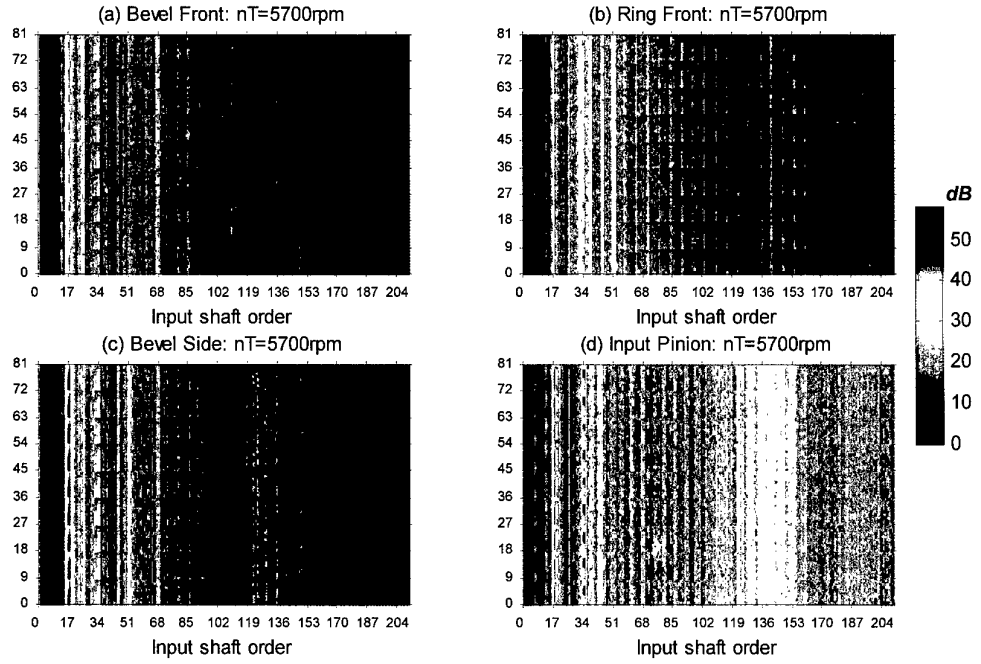

Figure 4-2. Power spectral images of the vibration signals at 95% speed (5700 rpm nT).

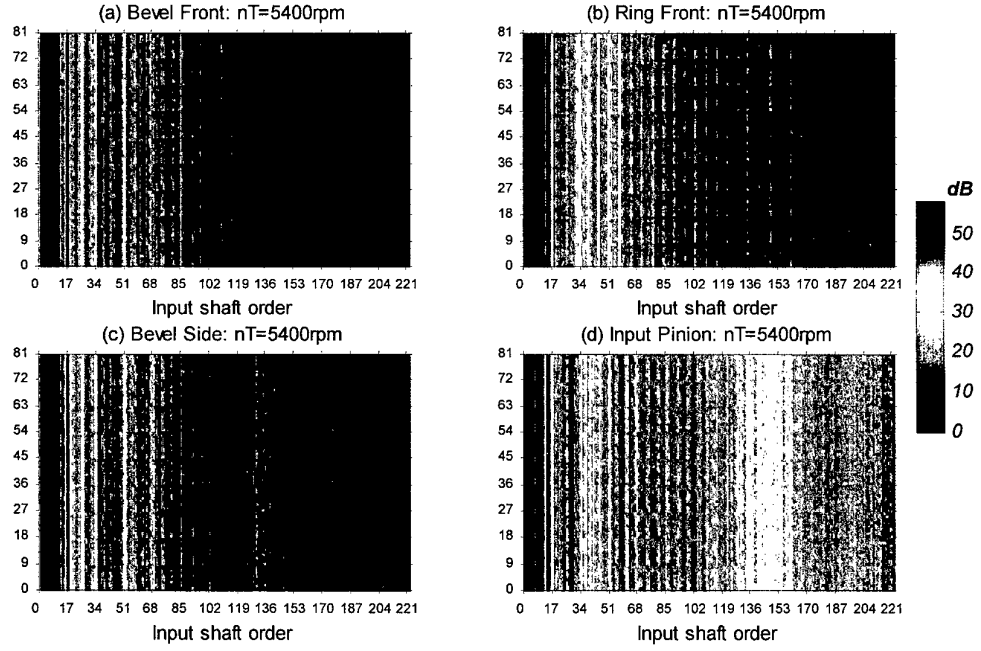

Figure 4-3. Power spectral images of the vibration signals at 90% speed (5400 rpm nT).

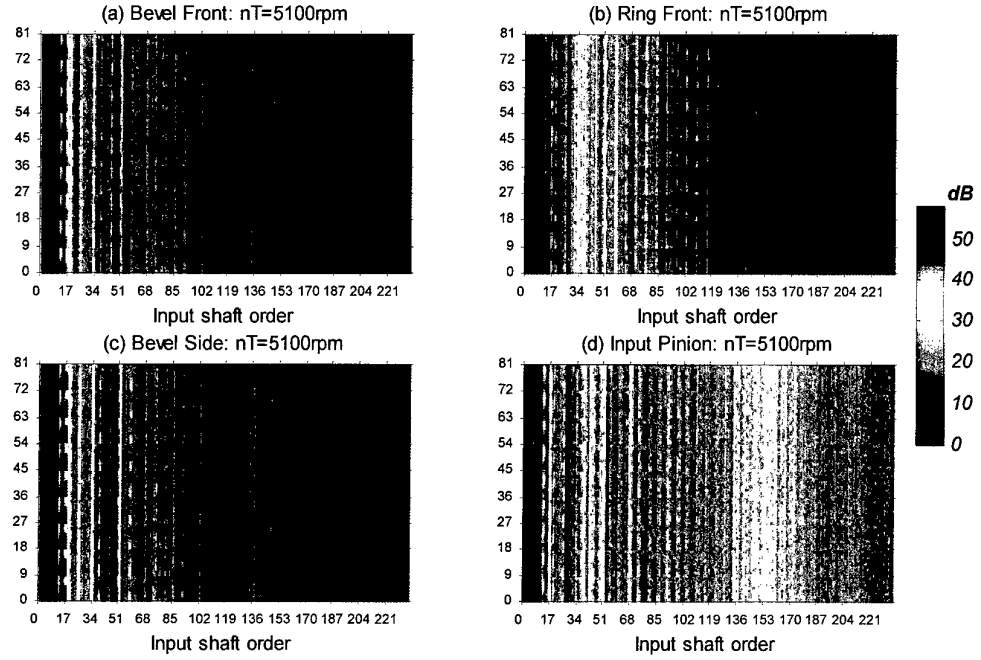

Figure 4-4. Power spectral images of the vibration signals at 85% speed (5100 rpm nT).

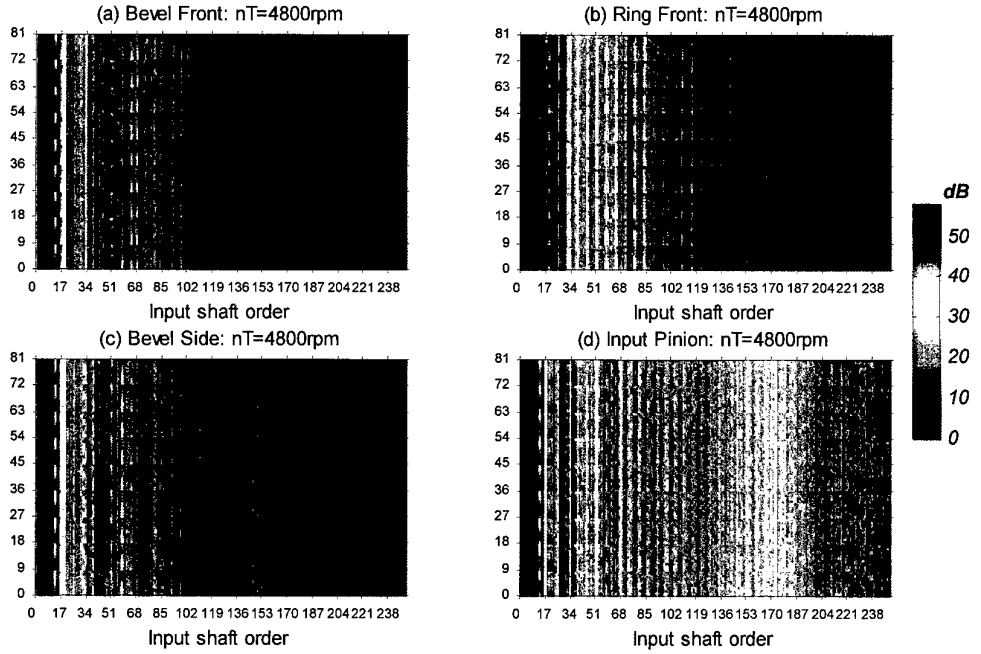

Figure 4-5. Power spectral images of the vibration signals at 80% speed (4800 rpm nT).

Figure 4-6 shows the amplitudes of the spectral component at the gear meshing frequency of the bevel gear stage for all four sensor-locations. These are sectional views of the spectral images shown in Figure 4-1 to Figure 4-4 at this frequency. It was found that both speed and sensor location produced significant effects on the range of these amplitudes. However, it was found that a higher speed did not necessarily correspond to a wider range of variation (Figure 4-6d). It was also found that at all locations except the Bevel-Front (Figure 4-6b, c and d) the amplitudes followed very regular patterns based on the 9 repetitive torques found in each RPL-stage (refer to Table 4-1). Thus, this spectral component was found to be less sensitive to the different mast loads at these locations. However, at the Bevel-Front location (Figure 4-6a), the patterns were less regular, especially at 95% speed (5700 rpm). Thus, the mast load produced a more significant effect at this location.

As the Ring-Front location is closer to the epicyclic stage, this was further examined. Figure 4-7 displays the high-power spectral components of the gear meshing harmonics of both the bevel gear stage (1st and 2nd harmonics), and the epicyclic stage (5th, 7th and 8th harmonics) at 100% speed (6000 rpm). The traces are sectional views of Figure 4-1b at the respective frequencies, but displayed on a linear scale. The variations in the spectral amplitudes caused by the different load conditions can be seen clearly in this figure. The highest power components of each gear mesh stage (i.e., the 2nd harmonic of the bevel stage, and the 5th harmonic of the epicyclic stage) varied substantially with mast load, and were probably the most mast-load dependent meshing harmonics for this gearbox. However, it should be noted that these variations only represented around 3dB on the logarithmic scale.

4.3 Waterfall Plots

Two waterfall plots of the power spectral images in section 4.1 are given in this section to further show the effects of load on the vibration of the AS 350B gearbox. In these plots, the x-axis is frequency, the y-axis is the load condition, and the z-axis is the power (g^2), although this is presented on a linear scale here instead of a logarithmic scale.

Figure 4-8 shows the waterfall plot of the power spectra at the Bevel-Side location at 95% speed (cf. Figure 4-2c). It can easily be seen that the dominant spectral component was the bevel gear meshing frequency (1615 Hz). The amplitude of this component varied with the repetitive torque conditions in each RPL-stage, and was slightly higher in the 4th, 5th, 8th and 9th RPL-stages (load conditions 28-36, 37-45, 64-72 and 73-81, respectively, in the figure) than those in the other RPL-stages. Also, it was just discernible that the components at the 2nd and 3rd harmonics of the bevel gear meshing frequency (3230 Hz & 4845 Hz) alternately emerged as the next most powerful component: the 2nd harmonic appeared under the higher torques, and the 3rd harmonic appeared under the lower torques.

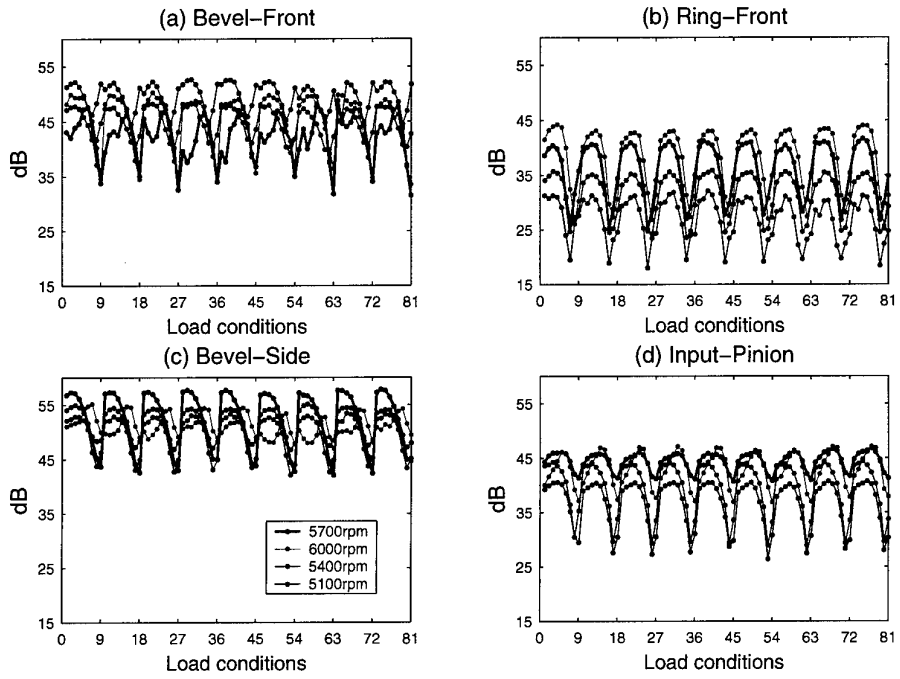

Figure 4-6. Spectral components at the bevel gear meshing frequency at all 4 sensor-locations.

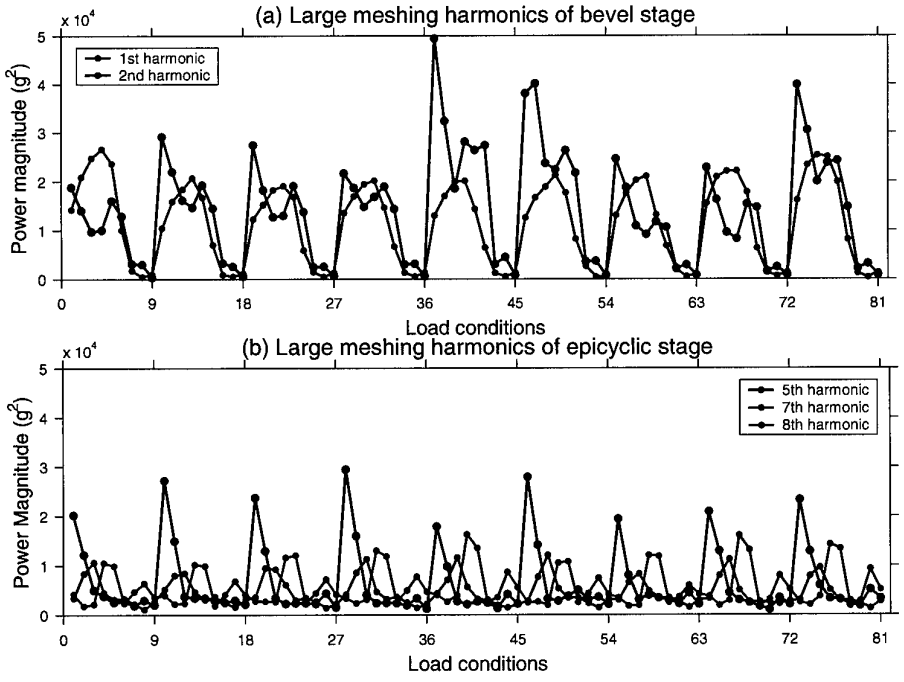

*Figure 4-7. Selected high-power spectral components (Ring-Front location, 100% speed) of gear meshing harmonics of: (**a**) the bevel gear stage, and (**b**) the epicyclic stage.*

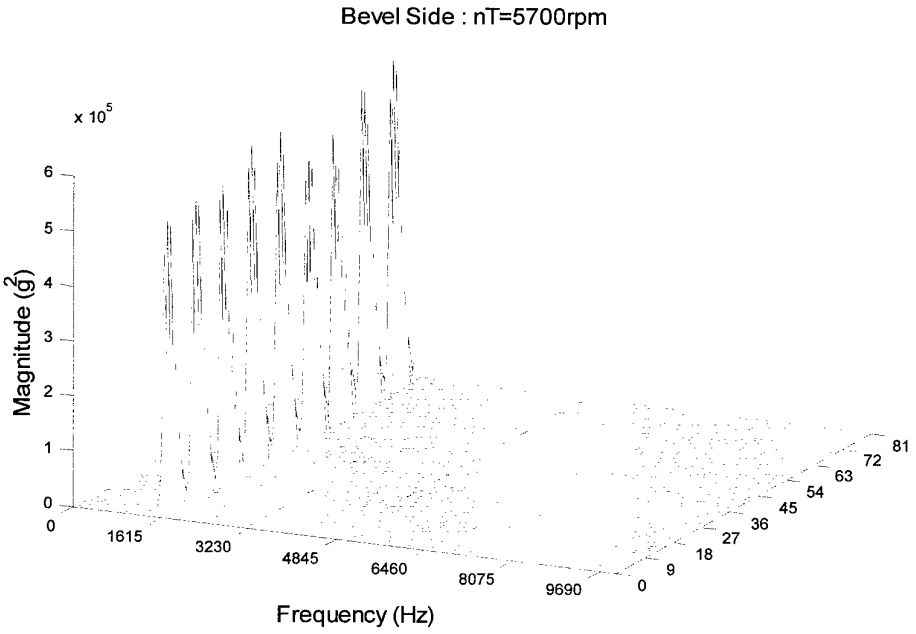

Figure 4-8. Waterfall plot of the vibration at the Bevel-side location at 95% speed (5700 rpm nT). Mesh frequencies: 1615 Hz for the bevel stage & 611.2Hz for the epicyclic stage.

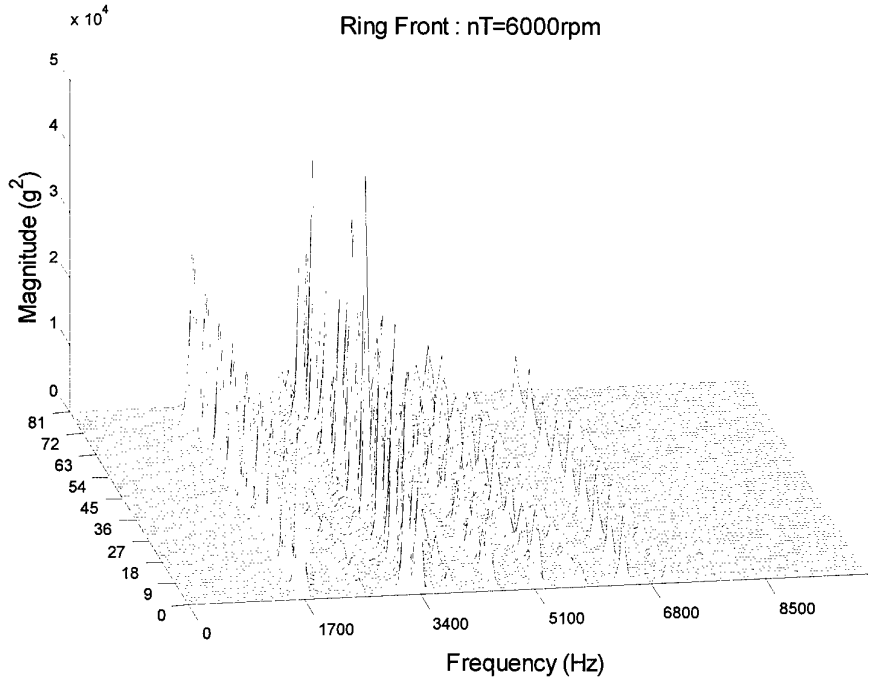

Figure 4-9. Waterfall plot of the vibration at the Ring-front location at 100% speed (6000 rpm nT). Mesh frequencies: 1700Hz for the bevel stage & 643.3Hz for the epicyclic stage.

Figure 4-9 shows the waterfall plot of the power spectra at the Ring-Front location at 100% speed (cf. Figure 4-1b). Because this location is closer to the epicyclic stage of the gearbox, the meshing harmonics of the epicyclic stage were stronger in appearance here. The plot is dominated by two series of gear meshing harmonics from the bevel-gear stage (×1700 Hz) and the epicyclic stage (×643 Hz). Because there are five planet gears in the epicyclic stage, it was not surprising that the 5th harmonic of the epicyclic stage (3216 Hz) emerged as the largest harmonic component from the epicyclic stage. Another noticeable fact was that the 7th and 10th meshing harmonics of the epicyclic stage (4502 Hz & 6431 Hz) were quite significant, and they behaved very differently to the torque variation.

4.4 Detailed Spectrum of the Vibration at the Ring-Front Location

A more detailed power spectrum of the vibration at a single location and load condition is presented here as an example of how the spectral components can be further resolved.

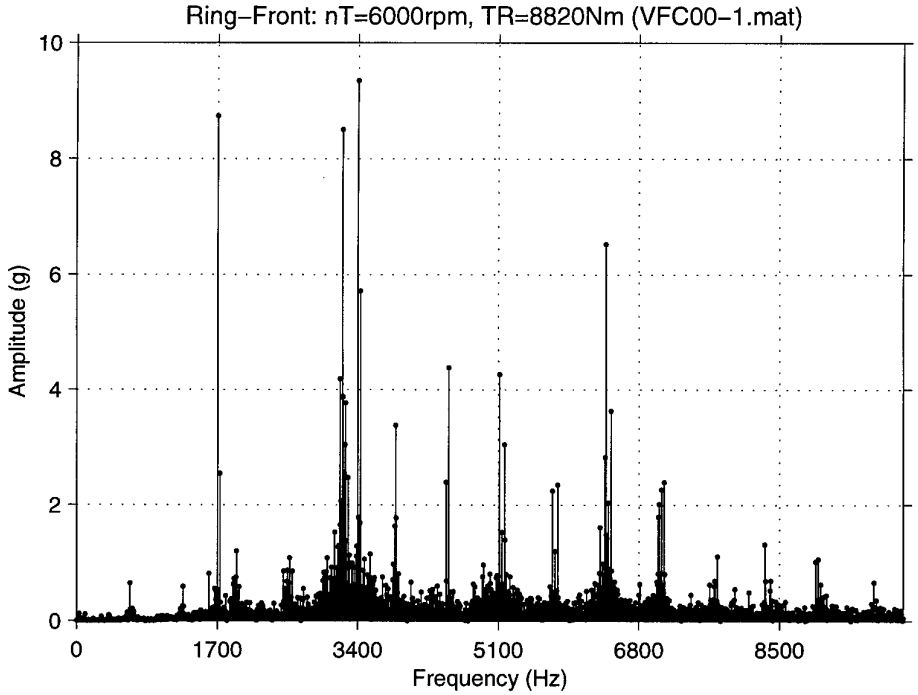

Figure 4-10. Power spectrum of the data from the Ring-Front location at 100% speed (6000rpm), 90% torque (TR=8820Nm), and zero mast load (RPL-Stage 1).

Figure 4-10 shows a power spectrum of the data from the Ring-Front location at 100% speed (6000 rpm nT), 90% torque (TR = 8820Nm), and zero mast load (RPL-Stage 1), where a much longer FFT length (8192-point) was used (cf. Figure 4-9 and Figure 4-1b,

load condition 1). It can be seen that the harmonic series from both the bevel gear and epicyclic stages are intertwined. The bevel stage series are dominated by the first two harmonics (1700 Hz & 3400 Hz), and each harmonic is surrounded by some modulation sidebands. The predominant components for the epicyclic stage series are the 5th and 10th harmonics (3216 Hz & 6431 Hz), which is to be expected since there are 5 planet gears in the gearbox.

4.5 Summary of Spectral Analyses

The major findings of the spectral analyses were:

- The meshing harmonics from the bevel gear stage were dominant at all four sensor-locations.
- The meshing harmonics from the epicyclic stage were relatively stronger at the Input-Pinion and, in particular, the Ring-Front locations.
- The first meshing harmonic of the bevel stage at the Bevel-Side location was the strongest component among all the sensor locations, and it was exceptionally large at 95% speed (5700 rpm nT).
- There was a structural resonance around 13600 Hz at the Input-Pinion location. The resonance was excited at all tested speeds by the higher-order gear meshing harmonics from both bevel and epicyclic stages.
- At 100% speed, the effects of mast load on the spectral content and harmonic magnitudes of the vibration data were far less significant than the effects of torque. However, further analysis of the effects of mast load on the vibration spectra of the AS 350B gearbox may need to be conducted.
- There were substantial effects from the torque on the power spectra of the vibration data, and these effects were different on different meshing harmonics.

5. Concluding Remarks

An investigation into the vibration characteristics of the Eurocopter AS 350B main rotor gearbox under different operating conditions was conducted at AMRL using the Helicopter Transmission Test Facility (HTTF). This investigation provided an understanding of the effects of different operating conditions on the vibration of the gearbox. From the analysis results, the following conclusions were drawn.

At the nominal operating speed of 6000 rpm, the overall RMS levels of gearbox vibration were predominantly affected by torque. Different mast loads only produced limited effects at three out of the four tested sensor locations. The tested sensor location that was most sensitive to the effects of mast load was the Bevel-Side location. However, at this location, the variation in the mast load only accounted for about 15% of the total variance of the vibration levels.

The investigation also found that the effects of torque on the spectral content of the vibration were substantial, and that these were location dependent. The effects of mast load on the spectral content of the vibration were limited. However, the effects of mast load in conjunction with the effect of a structural resonance identified near the Input-Pinion location may need to be further evaluated.

The lubricant pressure was strongly related to the operating speed of the gearbox. It was also slightly sensitive to the lubricant temperature, which varied between the thermostat settings of the electric fan on the oil cooler. It did not have a firm correlation with any other factors.

As dis-/re-assembly of gearboxes during maintenance actions can also introduce complex changes to their vibration features [1], further study on the effect of these actions should be conducted in the future.

6. Acknowledgments

The author would like to acknowledge Mr Ken Vaughan of AMRL for his assistance on the experimental work of the study, and Mr David Blunt, Dr Albert K. Wong, Mr Brian Rebbechi, and Dr B. David Forrester of AMRL for their support and comments on this study.

7. References

1. Huff, E M *et al* (2000), "Experimental Analysis of Mast Lifting and Bending Forces on Vibration Patterns Before and After Pinion Reinstallation in an OH-58 Transmission Test Rig", Proceedings of the American Helicopter Society 56th Annual Forum, Virginia Beach, Virginia, USA, May 2-4 2000.
2. Tabachnick, B G and Fidell, L S (1983), Using Multivariate Statistics, Harper & Row Publishers, New York.
3. Eurocopter France (1985), "AS 350B Main Rotor Gearbox Maintenance Manual".
4. RENK - Germany (1996), " Technical Manual of HTTF for AMRL ".

Appendix A: Sensor Locations and Force Directions

A.1. Vibration Sensor Locations

There were four accelerometers mounted on the casing of the AS 350B main gearbox during the VFC test. They were located on the gearbox casing near the bevel gear, the ring gear and the input shaft as shown in the following figures. The locations of these sensors are referred to here as Bevel-Front, Ring-Front, Bevel-Side and Input-Pinion, where 'Front' indicates the front of helicopter.

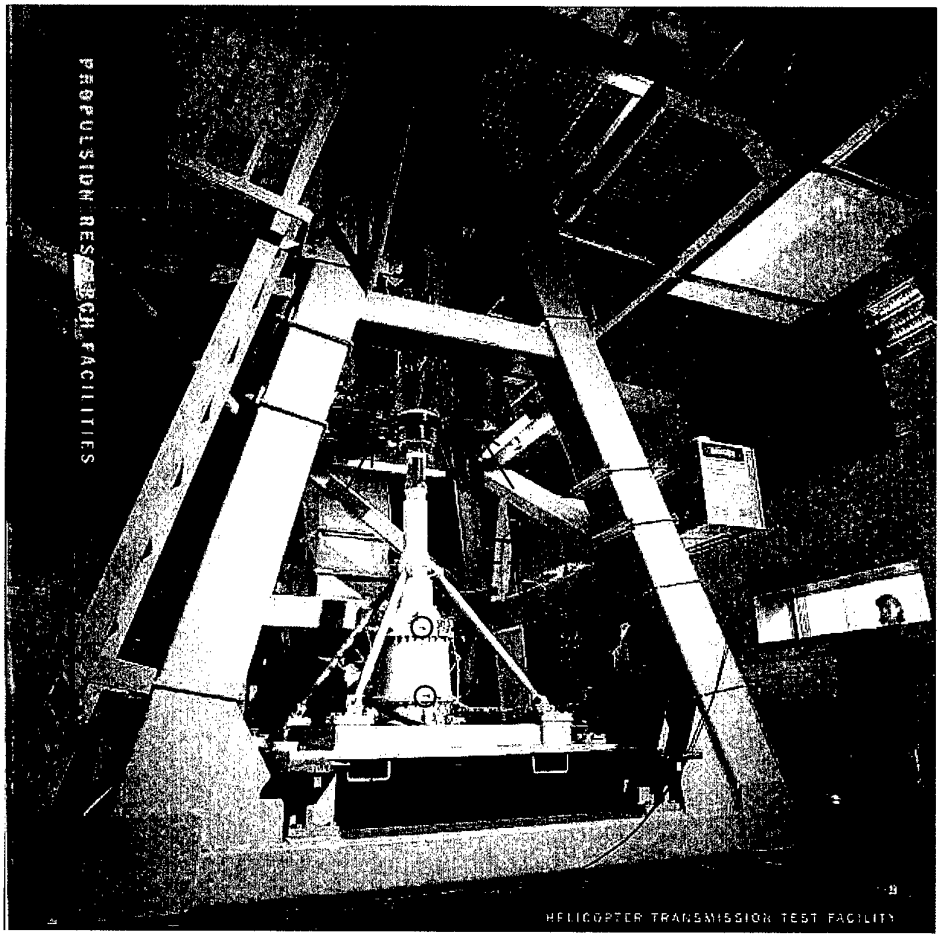

The above photograph shows the HTTF. The two red circles indicate the two front accelerometers (the top one is the Ring-Front and the bottom one is the Bevel-Front). The solid red arrows are pointing at the mast loading cylinders (one more vertical cylinder is invisible in the view) and the dashed red arrow is pointing at the upper bearing of the AS350B main gearbox. The following schematic diagrams (the views

from the input shaft and from the observation window of the control room) indicate the locations of the accelerometers.

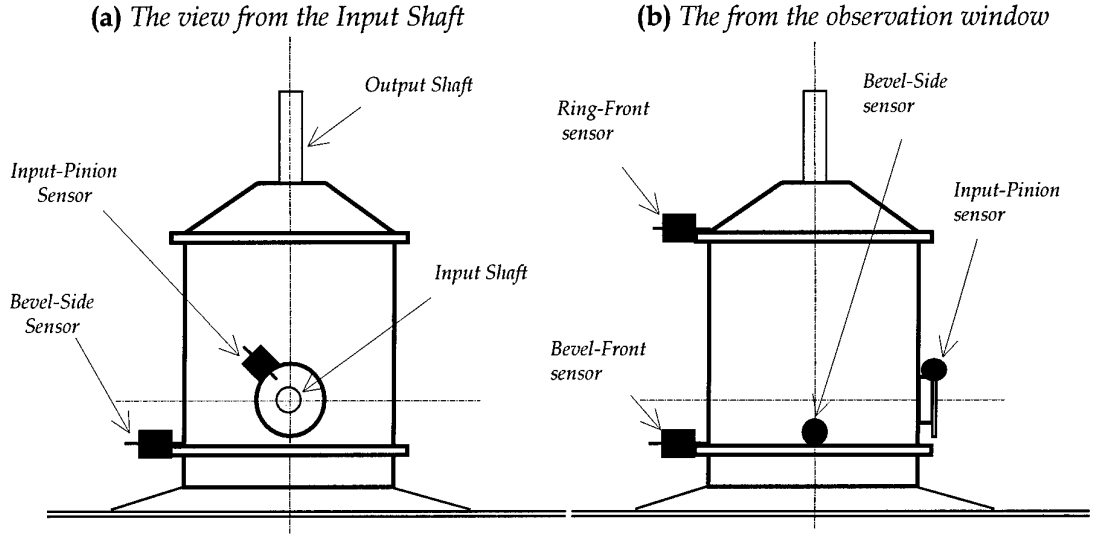

A.2. Horizontal Forces Applied to the Mast During the Test

Vjg"vqr"xkgy "qh"vjg"CU"572D"b ckp"igctdqz"*O ID+"ku"ujqyp"dgnqy<

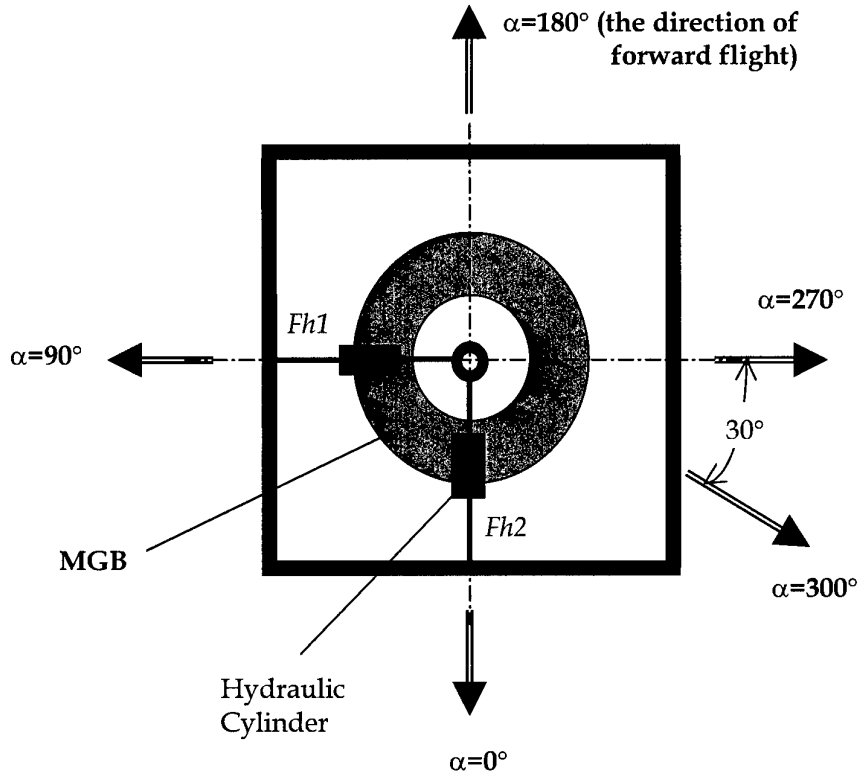

A.3. Helicopter Mast Loads

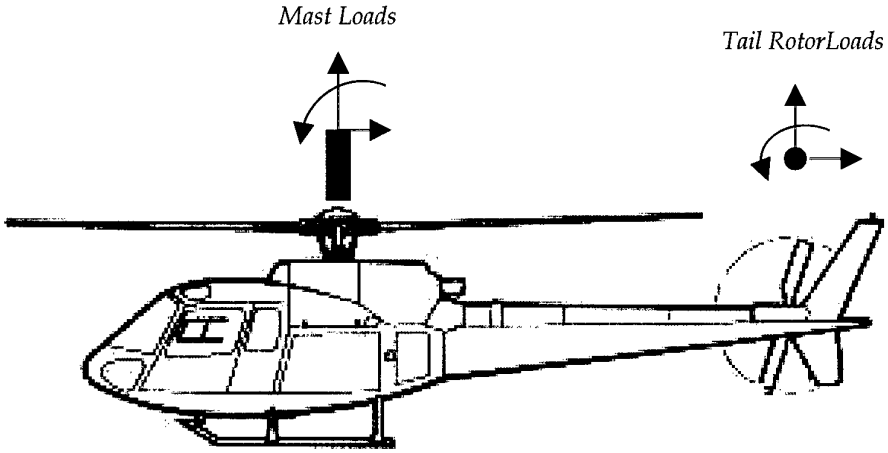

Appendix B: The Automatic Test Program

B.1. The RPG Programs

Table B-1 An example of the RPG programs

VFC00. RPG	Time			Set Value								
Stage	h	m	s	nT [rpm]	*d*nT [rpm/s]	TR [Nm]	*d*TR [Nm/s]	F_{ver} [N]	F_{hor} [N]	α [°]	Print [s]	Store [s]
1	**0**	**1**	**0**	**1500**	**100**	**500**	**400**	**0**	**0**	**0**	**60**	**60**
2	**0**	**1**	**0**	**3000**	**100**	**3000**	**400**	**0**	**0**	**0**	**60**	**60**
3	**0**	**1**	**0**	**4500**	**100**	**5000**	**400**	**0**	**0**	**0**	**60**	**60**
4	**0**	**10**	**0**	**6000**	**100**	**7000**	**400**	**0**	**0**	**0**	**60**	**60**
5	0	3	0	6000	100	8820	400	0	0	0	60	60
6	0	3	0	6000	100	7840	400	0	0	0	60	60
7	0	3	0	6000	100	6860	400	0	0	0	60	60
8	0	3	0	6000	100	5880	400	0	0	0	60	60
9	0	3	0	6000	100	4900	400	0	0	0	60	60
10	0	3	0	6000	100	3920	400	0	0	0	60	60
11	0	3	0	6000	100	2940	400	0	0	0	60	60
12	0	3	0	6000	100	1960	400	0	0	0	60	60
13	0	3	0	6000	100	980	400	0	0	0	60	60
14	0	3	0	5700	100	980	400	0	0	0	60	60
15	0	3	0	5700	100	1960	400	0	0	0	60	60
16	0	3	0	5700	100	2940	400	0	0	0	60	60
17	0	3	0	5700	100	3920	400	0	0	0	60	60
18	0	3	0	5700	100	4900	400	0	0	0	60	60
19	0	3	0	5700	100	5880	400	0	0	0	60	60
20	0	3	0	5700	100	6860	400	0	0	0	60	60
21	0	3	0	5700	100	7840	400	0	0	0	60	60
22	0	3	0	5700	100	8820	400	0	0	0	60	60
23	0	3	0	5400	100	8820	400	0	0	0	60	60
24	0	3	0	5400	100	7840	400	0	0	0	60	60
25	0	3	0	5400	100	6860	400	0	0	0	60	60
26	0	3	0	5400	100	5880	400	0	0	0	60	60
27	0	3	0	5400	100	4900	400	0	0	0	60	60
28	0	3	0	5400	100	3920	400	0	0	0	60	60
29	0	3	0	5400	100	2940	400	0	0	0	60	60
30	0	3	0	5400	100	1960	400	0	0	0	60	60
31	0	3	0	5400	100	980	400	0	0	0	60	60
32	0	3	0	5100	100	980	400	0	0	0	60	60
33	0	3	0	5100	100	1960	400	0	0	0	60	60

VFC00. RPG	Time			Set Value								
Stage	h	m	s	nT [rpm]	*d*nT [rpm/s]	TR [Nm]	*d*TR [Nm/s]	F_{ver} [N]	F_{hor} [N]	α [°]	Print [s]	Store [s]
34	0	3	0	5100	100	2940	400	0	0	0	60	60
35	0	3	0	5100	100	3920	400	0	0	0	60	60
36	0	3	0	5100	100	4900	400	0	0	0	60	60
37	0	3	0	5100	100	5880	400	0	0	0	60	60
38	0	3	0	5100	100	6860	400	0	0	0	60	60
39	0	3	0	5100	100	7840	400	0	0	0	60	60
40	0	3	0	5100	100	8820	400	0	0	0	60	60
41	0	3	0	4800	100	8820	400	0	0	0	60	60
42	0	3	0	4800	100	7840	400	0	0	0	60	60
43	0	3	0	4800	100	6860	400	0	0	0	60	60
44	0	3	0	4800	100	5880	400	0	0	0	60	60
45	0	3	0	4800	100	4900	400	0	0	0	60	60
46	0	3	0	4800	100	3920	400	0	0	0	60	60
47	0	3	0	4800	100	2940	400	0	0	0	60	60
48	0	3	0	4800	100	1960	400	0	0	0	60	60
49	0	3	0	4800	100	980	400	0	0	0	60	60
50	**0**	**1**	**0**	**2500**	**100**	**500**	**400**	**0**	**0**	**0**	**60**	**60**
51	**0**	**1**	**0**	**1000**	**100**	**200**	**400**	**0**	**0**	**0**	**60**	**60**
52	**0**	**2**	**0**	**0**	**100**	**0**	**400**	**0**	**0**	**0**	**60**	**60**

Note: (1) The stages highlighted in dark colour (1-4 and 50-52) are the warming up and run-down stages and data for these stages are not to be recorded.

(2) The last two columns did not play a part in our test.

(3) *d*nT and *d*TR are the change rate of nT (turbine input speed) and TR (rotor torque), respectively, during transition.

(4) The loading points of F_{hor} are 0.86m above the upper bearing of the gearbox.

Table B-2. Differences in F_{ver}, F_{hor} and α between VFC00.RPG and other .RPG files.

.RPG file name	Vertical Force	Horizontal Force	α
VFC00.RPG	*0*	*0*	*0°*
VFC50.RPG	*50% (10.3kN)*	*0*	*0°*
VFC55.RPG	*50% (10.3kN)*	*50% (1.0kN)*	*0°*
VFC5F.RPG	*50% (10.3kN)*	*100% (2.0kN)*	*0°*
VFCFF.RPG	*100% (20.6kN)*	*100% (2.0kN)*	*0°*
VFCFF1.RPG	*100% (20.6kN)*	*100% (2.0kN)*	*90°*
VFCFF2.RPG	*100% (20.6kN)*	*100% (2.0kN)*	*180°*
VFCFF3.RPG	*100% (20.6kN)*	*100% (2.0kN)*	*270°*
VFCFF4.RPG	*100% (20.6kN)*	*100% (2.0kN)*	*300°*

B.2. The RPL Program

Table B-3. The Renk-Program-Linker file: VFC.RPL

		RPL
RPL-Filename		*C:\AMRL\EXCEL\VFC.RPL*
RPL-set-cycles		**100**
RPL-Act-Cycles		**0 (updated during test)**
RPL-Act-Stage		**0 (updated during test)**
RPG-Act-Cycles		**0 (updated during test)**
RPG-Act-Stage		**0 (updated during test)**
RPG-Act-Hours		**0 (updated during test)**
RPG-Act-Minutes		**0 (updated during test)**
RPG-Act-Seconds		**0 (updated during test)**
RPL-Stage	**RPG-Cycles**	**RPG-Filename**
1	**1**	*C:\AMRL\EXCEL\VFC00.RPG*
2	**1**	*C:\AMRL\EXCEL\VFC50.RPG*
3	**1**	*C:\AMRL\EXCEL\VFC55.RPG*
4	**1**	*C:\AMRL\EXCEL\VFC5F.RPG*
5	**1**	*C:\AMRL\EXCEL\VFCFF.RPG*
6	**1**	*C:\AMRL\EXCEL\VFCFF1.RPG*
7	**1**	*C:\AMRL\EXCEL\VFCFF2.RPG*
8	**1**	*C:\AMRL\EXCEL\VFCFF3.RPG*
9	**1**	*C:\AMRL\EXCEL\VFCFF4.RPG*

B.3. Procedure for Running the HTTF under Automatic Mode

The procedure in generating the automatic test programs and running HTTF under the Automatic Mode are as follows:

- Open Renk program at USER level (press the Emergency STOP button to prevent the HTTF from running).
- In the Renk program window, choose Install → Change user level to SYSTEM level.
- Editor → Renk Program Generator (RPG), to edit the test program with Microsoft Excel (refer to Table B.1);
- RPG File → Compress, to compress the file then Save it as ***.RPG files.
- Close Renk Program Generator.
- Editor → Renk Program Linker (RPL), to edit the table with Excel. All values in the top half of the table except RPL-set-cycles are set to 0, the RPL-set-cycles field can be any positive integer (refer to Table B.3).

- RPL File → Compress, to compress the file then Save it as a ***.RPL file.
- Close Renk Program Linker.
- Test Bench Manager → Open AMRL350.con (or AMRL206.con for Bell 206 gearbox) file from the "aktcon" directory, to replace the last row in the table with the above edited ***.RPL file including its path, i.e. c:\AMRL\Excel\VFC.RPL.
- Click on Set as Test Bench to replace the previous AMRL350.con, then click OK.
- In the Renk window, choose Install → Change user level back to USER level.
- (Release the Emergency STOP button.) In Renk window, choose Test Mode → Automatic Run.

Appendix C: Description of Test Data

C.1. 16 Channels of Metrum Data

Table C-1. Channel setup on the Metrum recorder for the VFC test

Input Channel	Maximum Volts	Bandwidth (kHz)	Sampling Rate (kHz)	Annotation
1	5	40	160	Turbine Tacho 128/rev.
2	5	20	80	Turbine Tacho 1/rev. (nT)
3	5	5	20	Rotor Tacho 256/rev.
4	5	5	20	Rotor Tacho 1/rev. (nR)
5	2	20	80	Accelerometer, Bevel Gear – Front
6	2	20	80	Accelerometer, Ring Gear – Front
7	2	20	80	Accelerometer, Bevel Gear – Side
8	2	20	80	Accelerometer, Input Pinion
9	10	0.312	1.25	Lubricant Pressure
10	10	0.312	1.25	Mast Force, Vertical 1
11	10	0.312	1.25	Mast Force, Vertical 2
12	2	0.312	1.25	Mast Force, Horizontal 1
13	2	0.312	1.25	Mast Force, Horizontal 2
14	10	0.312	1.25	Lubricant Temperature
15	10	2.5	10	Turbine Torque (TT)
16	10	2.5	10	Rotor Torque (TR)

C.2. 10 Channels of Data (in Volts) Downloaded to MATLAB

Table C-2. Data from HTTF => Metrum (12-bit A/D & D/A) => HP E1432A (16-bit A/D)

Channel No.	Signal	Peak Voltage @ Metrum	Peak Voltage @ HP E1432A	Calibration
Ch1	Turbine 128/rev	5	2	×2.5
Ch2	Turbine 1/rev (***nT***)	5	2	×2.5
Ch3	Bevel front Vib (V_{BF})	2	2	10 mv/g
Ch4	Ring front Vib (V_{RF})	2	2	10 mv/g
Ch5	Bevel side Vib (V_{BS})	2	2	10 mv/g
Ch6	Input Pinion Vib (V_{IP})	2	2	10 mv/g
Ch7	Turbine Torque (***TT***)	10	2	(90 Nm/v) × 5
Ch8	Rotor Torque (***TR***)	10	2	(1300 Nm/v) × 5
Ch9	Lube Pressure (***LP***)	10	2	(100 kPa/v) × 5
Ch10	Lube Temp. (***LT***)	10	2	(15° C/v) × 5

Note: ×2.5 or ×5 are used to adjust the voltage changes from Metrum to HP E1432A

C.3. Description of file "Vib_Rms.mat" for RMS Analysis

This data file was generated by the Matlab program "VFC.m", it contains two variables, X and Y. The structures of X and Y are described as following:

X and Y are both multi-dimensional arrays:

$45 \times 4 \times 9 = N_{row} \times N_{column} \times N_{page}$

where N_{row} = Number of recorded stages for each .RPG file

N_{column} = Number of sub-variables

For X, the 4 sub-variables are the *mean values* of *TT, TR, LP* and *LT*.

For Y, the 4 sub-variables are the *RMS values* of V_{BF}, V_{RF}, V_{BS} and V_{IP}.

N_{page} = Number of combinations for F_{ver}, F_{hor}, and α, i.e. the RPL-Stages (refer to Table B-3)

The Following figures serve to depict the structures of X and Y graphically.

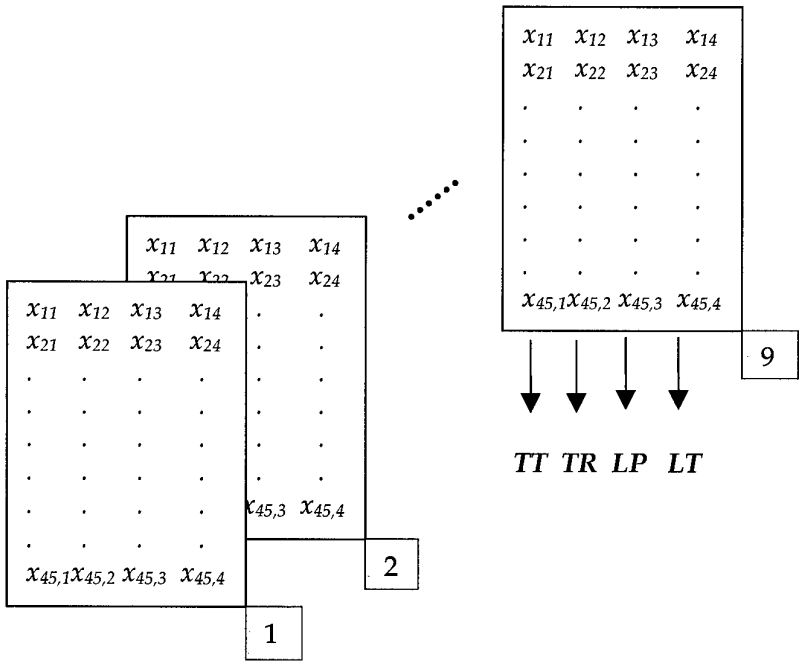

Figure C.1. The array structure for variable X.

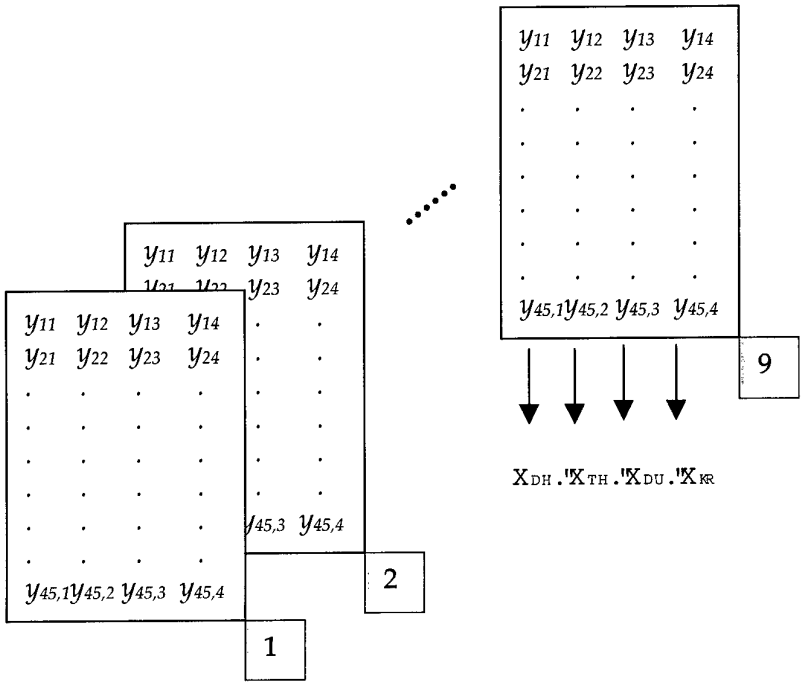

Figure C.2. The array structure for variable Y.

C.4. Description of file "Vib_**6000.mat" for ANOVA

There are 4 files, i.e. Vib_BS6000, Vib_IP6000, Vib_RF6000 and Vib_BF6000, which correspond to the RMS vibration levels at 4 sensor locations with the nominal operating speed (6000rpm nT). They were generated by program "VFC0.m". Each file contains a matrix with the dimension of 36 by 9, where the 36 rows correspond to 4 RMS levels of vibration for each of the 9 torques, and the 9 columns correspond to various mast loadings (i.e., the 9 RPL-stages shown in Table B-3). The following table serves to depict the structure of the matrices.

TR	Vfc00	Vfc50	...	VfcFF4
8820Nm (90% rated torque)	$V_{1,1}$ $V_{2,1}$ $V_{3,1}$ $V_{4,1}$	$V_{1,2}$ $V_{2,2}$ $V_{3,2}$ $V_{4,2}$	...	$V_{1,9}$ $V_{2,9}$ $V_{3,9}$ $V_{4,9}$
7840Nm (80%)	$V_{5,1}$ $V_{6,1}$ $V_{7,1}$ $V_{8,1}$	$V_{5,2}$ $V_{6,2}$ $V_{7,2}$ $V_{8,2}$	...	$V_{5,9}$ $V_{6,9}$ $V_{7,9}$ $V_{8,9}$
...	...	...	...	...
980Nm (10%)	$V_{33,1}$ $V_{34,1}$ $V_{35,1}$ $V_{36,1}$	$V_{33,2}$ $V_{34,2}$ $V_{35,2}$ $V_{36,2}$	...	$V_{33,9}$ $V_{34,9}$ $V_{35,9}$ $V_{36,9}$

One element with 4 replications

C.5. Description of file "Vib_PSD.mat" for Spectral Analysis

This data file was generated by program "VFC_spec.m". It contains two variables, the frequency f and the power spectral density P. The frequency (column) vector has 513 values that cover the frequency band of 25600Hz. The structure of variable P is described below (the graphic presentation of P is just a natural extension from 3D to 4D of the structures for variable X and Y in Appendix C.3):

P is a 4D array of 513×4×45×9, i.e. N_{row}×N_{column}×N_{page}×N_{room},
where N_{row} = (FFT-length)/2+1.
N_{column} = Number of vibration sensors, i.e. V_{BF}, V_{RF}, V_{BS} and V_{IP}.
N_{page} = Number of recorded stages for each RPG file.
N_{room} = Number of RPL-Stages (refer to Table B-3).

Appendix D: Analysis Programs

D.1. Matlab Program – VFC.m

```
% This program processes the Variable Flight Condition Data,
% generates "Vib_Rms.mat" data for function "Vfc_fig.m".
% Written by W. Wang, 3 April, 2000

clear

pp = 1          % start from page 1 (VFC test-file #1, ie. VFC00.RPG)
while pp < 10,
   if pp == 1,
      fname = 'f:\my_data\httf\variab~2\vfc_rpg\10chans\Vfc00\VFC00_';
   elseif pp == 2,
      fname = 'f:\my_data\httf\variab~2\vfc_rpg\10chans\Vfc50\VFC50_';
   elseif pp == 3,
      fname = 'f:\my_data\httf\variab~2\vfc_rpg\10chans\Vfc55\VFC55_';
   elseif pp == 4,
      fname = 'f:\my_data\httf\variab~2\vfc_rpg\10chans\Vfc5F\VFC5F_';
   elseif pp == 5,
      fname = 'f:\my_data\httf\variab~2\vfc_rpg\10chans\VfcFF\VFCFF_';
   elseif pp == 6,
      fname = 'f:\my_data\httf\variab~2\vfc_rpg\10chans\VfcFF1\VFCFF1_';
   elseif pp == 7,
      fname = 'f:\my_data\httf\variab~2\vfc_rpg\10chans\VfcFF2\VFCFF2_';
   elseif pp == 8,
      fname = 'f:\my_data\httf\variab~2\vfc_rpg\10chans\VfcFF3\VFCFF3_';
   else
      fname = 'f:\my_data\httf\variab~2\vfc_rpg\10chans\VfcFF4\VFCFF4_';
   end

   for kk=1:45,
      load([fname, num2str(kk)])

      % mean values of x-axes. Firstly, convert torque data to 'Nm', pressure
        to 'kPa' and temperature to 'degree C'
      x(kk,1:4) = mean([90*DATA_t(:,7), 1300*DATA_t(:,8), ...
                        100*DATA_t(:,9), 15*DATA_t(:,10)]);

      % RMS values for y-axes, convert vibration data to 'g'
      y(kk,1:4) = Rms(DATA_t(:,3:6)/0.01);
   end

   X(:,:,pp) = x;        % arrange it into a multi-dimensional (45*4*9) array
   Y(:,:,pp) = y;        % page 1 = 'VFC00', ... page 9 = 'VFCff4'.
   pp = pp + 1           % the next page

end

save f:\my_data\httf\variab~2\vfc_rpg\10chans\Vib_Rms X Y;
```

D.2. Matlab Program – VFC_fig.m

```
function Vfc_fig(pp)
% This program plots Figures from X & Y generated by Vfc.m
% Written by W. Wang, 4 April, 2000

load f:\my_data\httf\variab~2\vfc_rpg\10chans\Vib_Rms;

for kk = 1:5,
   figure(kk)

   plot(-X((kk-1)*9+(1:9),2,pp),Y((kk-1)*9+(1:9),4,pp),'x-')
   hold on
   plot(-X((kk-1)*9+(1:9),2,pp),Y((kk-1)*9+(1:9),3,pp),'ro-')
   plot(-X((kk-1)*9+(1:9),2,pp),Y((kk-1)*9+(1:9),2,pp),'gd-')
   plot(-X((kk-1)*9+(1:9),2,pp),Y((kk-1)*9+(1:9),1,pp),'ks-')

   ylabel('RMS Acceleration (g)')
   if     kk == 1, title('(a) nT = 6000 rpm')
   elseif kk == 2, title('(b) nT = 5700 rpm')
   elseif kk == 3, title('(c) nT = 5400 rpm')
   elseif kk == 4, title('(d) nT = 5100 rpm')
   else            title('(e) nT = 4800 rpm')
   end
   axis([500 9500 0 50])
end

xlabel('Rotor Torque (actual average value, in Nm)')
legend('Input pinion', 'Bevel, side','Ring, front','Bevel, front')
```

D.3. Matlab Propram – Anova_2.m

```
function p = anova_2(X,reps)
%
% ANOVA_2 Two-way analysis of variance.
%   ANOVA_2(X,REPS) performs a balanced two-way ANOVA for comparing the
%   means of two or more columns and two or more rows of the sample in X.
%   The data in different columns represent changes in one factor. The data
%   in different rows represent changes in the other factor. If there is
%   more than one observation per row-column pair, then the argument, REPS,
%   indicates the number of observations per "cell". A cell contains REPS
%   number of rows.
%
%   For example, if REPS = 3, then each cell contains 3 rows and the total
%   number of rows must be a multiple of 3. If X has 12 rows, and REPS = 3,
%   then the "row" factor has 4 levels (3*4 = 12). The second level of the
%   row factor goes from rows 4 to 6.
%
%   p  - the probabilities of F's given equal column/row means, no
%  interaction.

%   Modified from "anova2" in Matlab statistics toolbox, 19 May 2000.

[r,c] = size(X);
if nargin == 1,
  reps = 1;
  m=r;
  Y = X;
elseif reps == 1
  m=r;
  Y = X;
else
  m = r/reps;              % m is the number of cells
  if (floor(m) ~= r/reps),
      error('The number of rows must be a multiple of reps.');
  end
```

```
  Y = zeros(m,c);
  for i=1:m,
      j = (i-1)*reps;
      Y(i,:) = mean(X(j+1:j+reps,:));
  end
end

colmean = mean(Y);              % column means
rowmean = mean(Y');             % row means
gm = mean(colmean);             % grand mean
df1 = c-1;                      % Column degrees of freedom
df2 = m-1;                      % Row degrees of freedom
if reps == 1,
   % Error degrees of freedom. No replication. This assumes an additive model.
  edf = (c-1)*(r-1);
else
  edf = (c*m*(reps-1));         % Error degrees of freedom with replicates
  idf = (c-1)*(m-1);            % Interaction degrees of freedom
end
CSS = m*reps*(colmean - gm)*(colmean-gm)';              % Column Sum of
Squares
RSS = c*reps*(rowmean - gm)*(rowmean-gm)';              % Row Sum of Squares
correction = (c*m*reps)*gm^2;
TSS = sum(sum(X .* X)) - correction;                    % Total Sum of Squares
ISS = reps*sum(sum(Y .* Y)) - correction - CSS - RSS;   % Interaction Sum of
Squares
if reps == 1,
  SSE = ISS;
else
  SSE = TSS - CSS - RSS - ISS;          % Error Sum of Squares
end

if (SSE~=0)
    MSE  = SSE/edf;
    colf = (CSS/df1) / MSE;
    rowf = (RSS/df2) / MSE;
    colp = 1 - fcdf_0(colf,df1,edf);  % Probability of F given equal column
means.
    rowp = 1 - fcdf_0(rowf,df2,edf);  % Probability of F given equal row
means.
    p    = [colp rowp];

    if (reps > 1),
       intf = (ISS/idf)/MSE;
       ip   = 1 - fcdf_0(intf,idf,edf); % Probability of F given no
interaction
       p    = [p ip];
    end

else                    % Dealing with special cases around no error.

    if CSS==0,          % No between column variability.
      colf = 0;
      colp = 1;
    else                % Between column variability.
      colf = Inf;
      colp = 0;
    end

    if RSS==0,          % No between row variability.
      rowf = 0;
      rowp = 1;
    else                % Between row variability.
      rowf = Inf;
      rowp = 0;
    end

    p = [colp rowp];
```

```
    if (reps>1) & (ISS==0)  % Replication but no interactions.
      intf = 0;
      p = [p 1];
    elseif (reps>1)         % Replication with interactions.
      intf = Inf;
      p = [p 0];
    end
end

if (reps > 1),
  numrows = 5;
  Table=zeros(numrows,4);   %Formatting for ANOVA Table printout with
interactions.
  Table(:,1)=[ CSS RSS ISS SSE TSS]';
  Table(:,2)=[df1 df2 idf edf r*c-1]';
  Table(:,3)=[ CSS/df1 RSS/df2 ISS/idf SSE/edf Inf ]';
  Table(:,4)=[ colf rowf intf Inf Inf ]';
else
  numrows = 4;
  Table=zeros(4,4);         % Formatting for ANOVA Table printout no
interactions.
  Table(:,1)=[ CSS RSS SSE TSS]';
  Table(:,2)=[df1 df2 edf r*c-1]';
  Table(:,3)=[ CSS/df1 RSS/df2 SSE/edf Inf ]';
  Table(:,4)=[ colf rowf Inf Inf ]';
end

figh = figure('pos', [50 350 500 300]);
z0 = 0.00;
y0 = 0.85;
dz = 0.15;
dy =0.06;
text(z0+0.40,y0,'ANOVA Table')
axis off

z=z0+dz;
y=y0-3*dy/2;
colheads = ['Source      ';'         SS ';'          df';'       MS   ';...
            '          F '];

for i=1:5
  text(z,y,colheads(i,:))
  z = z + dz;
end
drawnow
if numrows == 5,
  rowheads = ['Columns  ';'Rows     ';'Interaction';'Error     ';'Total    '];
else
  rowheads = ['Columns  ';'Rows     ';'Error      ';'Total     '];
end
for i=1:numrows
  y = y0-(i+1.5)*dy;
  z = z0 + dz;
  h = text(z,y,rowheads(i,:));

  z = z + dz;
  for j=1:4
    if (Table(i,j) ~= Inf) & j ~=2,
      h = text(z,y,sprintf('%10.4g',Table(i,j)));
      z = z + dz;
    elseif j==2,
      z = z + dz/4;
      h = text(z,y,sprintf('%7.5g',Table(i,j)));
      z = z + 3*dz/4;
    end
  end
  drawnow
end
```

D.4. Matlab Propram – VFC_spec.m

```
% This program calculates the PSD of the VFC data & save it as Vib_PSD.mat
% Written by W. Wang, 10 April 2000

clear
rr = 1              % start from room 1 (VFC test-file #1, ie. VFC00.RPG)
while rr < 10,
   if rr == 1,
      fname = 'f:\my_data\httf\variab~2\vfc_rpg\10chans\Vfc00\VFC00_';
   elseif rr == 2,
      fname = 'f:\my_data\httf\variab~2\vfc_rpg\10chans\Vfc50\VFC50_';
   elseif rr == 3,
      fname = 'f:\my_data\httf\variab~2\vfc_rpg\10chans\Vfc55\VFC55_';
   elseif rr == 4,
      fname = 'f:\my_data\httf\variab~2\vfc_rpg\10chans\Vfc5F\VFC5F_';
   elseif rr == 5,
      fname = 'f:\my_data\httf\variab~2\vfc_rpg\10chans\VfcFF\VFCFF_';
   elseif rr == 6,
      fname = 'f:\my_data\httf\variab~2\vfc_rpg\10chans\VfcFF1\VFCFF1_';
   elseif rr == 7,
      fname = 'f:\my_data\httf\variab~2\vfc_rpg\10chans\VfcFF2\VFCFF2_';
   elseif rr == 8,
      fname = 'f:\my_data\httf\variab~2\vfc_rpg\10chans\VfcFF3\VFCFF3_';
   else
      fname = 'f:\my_data\httf\variab~2\vfc_rpg\10chans\VfcFF4\VFCFF4_';
   end

   for kk=1:45,
      load([fname, num2str(kk)])
      % convert vibration data to 'g', calculate PSD
      Pyy(1:513,1) = psd(DATA_t(:,3)/0.01,1024,51200,[],512);
      Pyy(1:513,2) = psd(DATA_t(:,4)/0.01,1024,51200,[],512);
      Pyy(1:513,3) = psd(DATA_t(:,5)/0.01,1024,51200,[],512);
      Pyy(1:513,4) = psd(DATA_t(:,6)/0.01,1024,51200,[],512);
      Pk(:,:,kk) = Pyy;
   end
   P(:,:,:,rr) = Pk;      % room 1 = 'VFC00', ... room 9 = 'VFCff4'.
   rr = rr + 1            % the next room
end
% P is dimensioned by 513*4*45*9 = NFFT/2+1 * 4_Sensors * 45_Records *
% 9_Conditions.

f = (0:1023)*51200/1024; f = f(1:513)';
save f:\my_data\httf\variab~2\vfc_rpg\10chans\Vib_PSD f P;
```

D.5. Matlab Program – VfcS_fig.m

```
function VfcS_fig(nT,sensor)
% This program plots (IMAGESC) the power spectral images using the VFC
% vibration spectral data stored in the file "Vib_PSD.mat" generated by
% program Vfc_spec.m
%
%     nT = 6000rpm
%     nT = 5700rpm
%     nT = 5400rpm
%     nT = 5100rpm
%     nT = 4800rpm
%
% sensor = 1: Bevel Front
% sensor = 2: Ring  Front
% sensor = 3: Bevel Side
% sensor = 4: Input Pinion
```

```
%
%     rr = 1: the spectral data is from  'Vfc00.rpg', room 1
%         ...                             ...
%     rr = 9: the spectral data is from 'VfcFF4.rpg', room 9

% Written by W. Wang, 11 April, 2000

% load spectral data f and P, P is dimensioned by
% 513*4*45*9 = (NFFT/2+1) * 4_Sensors * 45_Recorded_stages *
% 9_Conditions.

load f:\my_data\httf\variab~2\vfc_rpg\10chans\Vib_PSD

sname = ['Bevel Front '; ' Ring Front '; ' Bevel Side '; 'Input Pinion'];
fband = 20000;
fmax = find(f==fband);
xt = nT/60*17;                          % xtick at meshing frequency
if     nT == 6000, k = 1;
elseif nT == 5700, k = 2;
elseif nT == 5400, k = 3;
elseif nT == 5100, k = 4;
elseif nT == 4800, k = 5;
else error('Wrong nT !!! nT should be one of these values: ...
            6000,5700,5400,5100,4800')
end

ZZ = [];
for rr = 1:9,                           % room number
   Z(1:fmax,1:9) = P(1:fmax,sensor,(k-1)*9+(1:9),rr);
   % make sure a descending TR (8820Nm -> 980Nm)
   if k == 2 | k == 4, Z = fliplr(Z); end
   ZZ = [ZZ Z];
end
ZdB = 10*log10(ZZ');
% 57.77dB is found maximum with nT=5700rpm & Bevel-Side sensor
figure(1), imagesc( f(1:fmax), 0:81, ZdB, [0 58] ), axis xy
set(gca,'xtick',[0:xt:fband],'ylim',[0 81],'ytick',[0:9:81],'tick','out')

title([sname(sensor,:), ': nT=', num2str(nT), 'rpm']),
xlabel('Frequency (Hz)')
```

DISTRIBUTION LIST

An Investigation of the Vibration Characteristics of the Eurocopter AS 350B Main Rotor Gearbox Under Different Operating Conditions

Wenyi Wang

AUSTRALIA

DEFENCE ORGANISATION

Task Sponsor Chief Airframes and Engines Division, DSTO

S&T Program

Chief Defence Scientist
FAS Science Policy
AS Science Corporate Management
Director General Science Policy Development
} shared copy

Counsellor Defence Science, London (Doc Data Sheet)
Counsellor Defence Science, Washington (Doc Data Sheet)
Scientific Adviser to MRDC Thailand (Doc Data Sheet)
Scientific Adviser Joint
Navy Scientific Adviser (Doc Data Sheet and distribution list only)
Scientific Adviser - Army (Doc Data Sheet and distribution list only)
Air Force Scientific Adviser
Director Trials

Aeronautical and Maritime Research Laboratory

Director
Chief of Airframes and Engines Division
Research Leader Propulsion
Task Manager: B.D. Forrester
Author: W. Wang (5 copies)
A.K. Wong
D. Blunt
B. Rebbichi
M. Shilo
A. Becker
P. Marsden
T. Galati
K. Vaughan
G. Forsyth
P. Frith

DSTO Library and Archives

Library Fishermans Bend (Doc Data Sheet)
Library Maribyrnong (Doc Data Sheet)
Library Salisbury
Australian Archives

Library, MOD, Pyrmont (Doc Data sheet only)
US Defense Technical Information Center, 2 copies
UK Defence Research Information Centre, 2 copies
Canada Defence Scientific Information Service, 1 copy
NZ Defence Information Centre, 1 copy
National Library of Australia, 1 copy

Capability Development Division
Director General Maritime Development (Doc Data Sheet only)
Director General Aerospace Development (Doc Data Sheet only)

Knowledge Staff
Director General Command, Control, Communications and Computers (DGC4) (Doc Data Sheet only)

Navy
SO (Science), Director of Naval Warfare, Maritime Headquarters Annex, Garden Island, NSW 2000. (Doc Data Sheet only)
AS 350B Logistics Manager, NASPO, HMAS Albatross, Nowra NSW 2540.

Army
Stuart Schnaars, ABCA Standardisation Officer, Tobruk Barracks, Puckapunyal, 3662 (4 copies)
SO (Science), Deployable Joint Force Headquarters (DJFHQ) (L), MILPO Gallipoli Barracks, Enoggera QLD 4052 (Doc Data Sheet only)
NPOC QWG Engineer NBCD Combat Development Wing, Tobruk Barracks, Puckapunyal, 3662 (Doc Data Sheet relating to NBCD matters only)
COMD, Headquarters Aviation Support Group, Army Aviation Centre, Army Airfield, Oakey, QLD 4401

Air Force
Tech Reports, CO Engineering Squadron, Aircraft Research and Development Unit, RAAF Base Edinburgh, SA 5111
SCI4A, DGTA, RAAF Base Williams, Laverton VIC 3027.

Intelligence Program
DGSTA Defence Intelligence Organisation
Defence Intelligence Organisation-Information Centre

Corporate Support Program
Library Manager, DLS-Canberra

UNIVERSITIES AND COLLEGES
Australian Defence Force Academy
Library
Head of Aerospace and Mechanical Engineering
Serials Section (M list), Deakin University Library, Geelong, 3217 (
Senior Librarian, Hargrave Library, Monash University
Librarian, Flinders University
A/Prof. R.B. Randall, School of Mechanical and Manufacturing Engineering, University of New South Wales, Sydney, NSW 2052

Prof. J. Mathew, School of Mechanical and Manufacturing Engineering, Queensland University of Technology, GPO Box 2434, Brisbane, QLD 4001

Dr. I.M. Howard, Department of Mechanical Engineering, Curtin University of Technology, GPO Box U1987, Perth, WA 6001

OTHER ORGANISATIONS

NASA (Canberra)

AusInfo

OUTSIDE AUSTRALIA

ABSTRACTING AND INFORMATION ORGANISATIONS

Library, Chemical Abstracts Reference Service

Engineering Societies Library, US

Materials Information, Cambridge Scientific Abstracts, US

Documents Librarian, The Center for Research Libraries, US

INFORMATION EXCHANGE AGREEMENT PARTNERS

Acquisitions Unit, Science Reference and Information Service, UK

Library - Exchange Desk, National Institute of Standards and Technology, US

THE TECHNICAL COOPERATION PROGRAM (TTCP)

Technical Panel AER-TP3, Propulsive and Mechanical Systems Condition Monitoring and Diagnostics

Mr. A. Hess, Naval Air Warfare Center - Aircraft Division, Building 106 Unit 4, 22195 Elmer Road, Patuxent River MD 20670-1534, USA

Mr W.J. Hardman, Naval Air Warfare Center - Aircraft Division, Building 106 Unit 4, 22195 Elmer Road, Patuxent River MD 20670-1534, USA.

Mr J. Bird, Structures Materials & Propulsion Laboratory, National Research Council Canada, Institute for Aerospace Research, Building M-7, Montreal Road, Ottawa, Ontario K1A 0R6, Canada.

Mr P. Conor, Defence Scientific Establishment, NZ Defence Force, Auckland Naval Base, Auckland, New Zealand.

UK National Leader

Other Organisations

Mr. Patrice Samon, Direction Programme Recherches, Avionique et système, Eurocopter France, 13725 Marignane Cedex, France

SPARES 10

Total number of copies: **75**

DEFENCE SCIENCE AND TECHNOLOGY ORGANISATION
DOCUMENT CONTROL DATA

1. PRIVACY MARKING/CAVEAT (OF DOCUMENT)

2. TITLE

An Investigation of the Vibration Characteristics of the Eurocopter AS350B Main Rotor Gearbox Under Different Operating Conditions

3. SECURITY CLASSIFICATION (FOR UNCLASSIFIED REPORTS THAT ARE LIMITED RELEASE USE (L) NEXT TO DOCUMENT CLASSIFICATION)

Document	(U)
Title	(U)
Abstract	(U)

4. AUTHOR(S)

Wenyi Wang

5. CORPORATE AUTHOR

Aeronautical and Maritime Research Laboratory
506 Lorimer St
Fishermans Bend Vic 3207 Australia

6a. DSTO NUMBER	6b. AR NUMBER	6c. TYPE OF REPORT	7. DOCUMENT DATE
DSTO-TR-1217	AR-012-029	Technical Report	October 2001

8. FILE NUMBER	9. TASK NUMBER	10. TASK SPONSOR	11. NO. OF PAGES	12. NO. OF REFERENCES
M1/9/804	NAV 98/094	DGTA	44	4

13. URL on the World Wide Web

http://www.dsto.defence.gov.au/corporate/reports/DSTO-TR-1217.pdf

14. RELEASE AUTHORITY

Chief, Airframes and Engines Division

15. SECONDARY RELEASE STATEMENT OF THIS DOCUMENT

Approved for public release

OVERSEAS ENQUIRIES OUTSIDE STATED LIMITATIONS SHOULD BE REFERRED THROUGH DOCUMENT EXCHANGE, PO BOX 1500, SALISBURY, SA 5108

16. DELIBERATE ANNOUNCEMENT

No Limitations

17. CASUAL ANNOUNCEMENT Yes

18. DEFTEST DESCRIPTORS

Helicopter transmission, Eurocopter AS 350B, Operating condition, Vibration analysis

19. ABSTRACT

Different flight conditions can introduce complex changes to the vibration of helicopter transmissions, which may cause a vibration-based in-flight transmission diagnostic system to produce false alarms. An investigation into the vibration characteristics of the Eurocopter AS 350B main rotor gearbox under different operating conditions was conducted at AMRL. This investigation provided some in-depth understanding of the effects of different operating conditions, such as speed, torque and mast load, on the vibration of the gearbox. The analysis results showed that the effects of torque load were predominant and were dependent on operating speed and sensor locations, but that the effects of mast load were limited at most sensor locations. At the sensor location near the input shaft, the effects of torque and mast load on the vibration of the AS 350B gearbox were minimal.

TECHNICAL MEMORANDUM DSTO-TM-1421 AUGUST 2004

DEPARTMENT OF DEFENCE
DEFENCE SCIENCE & TECHNOLOGY ORGANISATION
DSTO

AERONAUTICAL AND MARITIME RESEARCH LABORATORY
506 LORIMER STREET FISHERMANS BEND VICTORIA 3207 AUSTRALIA
TELEPHONE (03) 9626 7000